Title	Redox-responsive mesoporous silica nanoparticles : a physiologically sensitive codelivery vehicle for siRNA and doxorubicin
Author(s)	Ma, Xing; Teh, Cathleen; Zhang, Quan; Borah, Parijat; Choong, Cleo Swee Neo; Korzh, Vladimir; Zhao, Yanli
Citation	Ma, X., Teh, C., Zhang, Q., Borah, P., Choong, C. S. N., Korzh, V., et al. (2014). Redox-responsive mesoporous silica nanoparticles : a physiologically sensitive codelivery vehicle for siRNA and doxorubicin. Antioxidants & redox signaling, 21(5), 707-722.
Date	2014
URL	http://hdl.handle.net/10220/25156
Rights	© 2014 Mary Ann Liebert. This paper was published in Antioxidants & Redox Signaling and is made available as an electronic reprint (preprint) with permission of Mary Ann Liebert. The paper can be found at the following official DOI: [http://dx.doi.org/10.1089/ars.2012.5076]. One print or electronic copy may be made for personal use only. Systematic or multiple reproduction, distribution to multiple locations via electronic or other means, duplication of any material in this paper for a fee or for commercial purposes, or modification of the content of the paper is prohibited and is subject to penalties under law.

ANTIOXIDANTS & REDOX SIGNALING
Volume 21, Number 5, 2014

DOI: 10.1089/ars.2012.5076

Therapeutics

FORUM ORIGINAL RESEARCH COMMUNICATION

Redox-Responsive Mesoporous Silica Nanoparticles: A Physiologically Sensitive Codelivery Vehicle for siRNA and Doxorubicin

Xing Ma,[1,2] Cathleen Teh,[3] Quan Zhang,[1] Parijat Borah,[1] Cleo Choong,[2] Vladimir Korzh,[3,4] and Yanli Zhao[1,2]

Abstract

Aims: Efficient siRNA/drug codelivery carriers can offer great promises to cancer treatment on account of synergistic effect provided from cancer-associated gene and anticancer drugs. In this work, a redox-responsive drug/siRNA codelivery vehicle based on mesoporous silica nanoparticles was fabricated to simultaneously deliver siRNA and doxorubicin (Dox) *in vitro* and *in vivo*. ***Results:*** The nanoparticle surface was functionalized with the adamantane (AD) units. Formation of stable host–guest complex between disulfide bond linked-AD and ethylenediamine-modified β-cyclodextrin is capable of fully blocking drugs inside the nanopores, while amino groups can complex with siRNA *via* electrostatic interaction. Relatively high concentration of glutathione in biophysical environment provides natural reducing agent to trigger drug/siRNA release by cleaving pre-introduced disulfide bonds. B-cell lymphoma 2 (*Bcl-2*) siRNA was codelivered to silence *Bcl-2* protein expression in HeLa cells, resulting in enhanced chemotherapy efficacy *in vitro*. *In vivo* delivery experiment carried out in transgenic zebrafish larvae indicates that the delivery of Dox inhibits the development of choroid plexus in a dose-dependent manner, leading to successful decrease of green fluorescence protein transcription in choroid plexus. Reduction of liver tumor was also demonstrated after injection of Dox-loaded nanoparticles. ***Innovation:*** We successfully demonstrated that functional nanoparticles could serve as an efficient carrier for the delivery of *Bcl-2* siRNA and Dox in HeLa cells and in transgenic zebrafish larvae, leading to enhanced therapeutic efficacy. ***Conclusion:*** Enhanced cytotoxicity caused by simultaneous delivery of *Bcl-2* siRNA and Dox was observed in HeLa cells. Drug-loaded nanoparticles were internalized *in vivo*, inhibiting the development of choroid plexus and the progression of liver tumor. *Antioxid. Redox Signal.* 21, 707–722.

Introduction

An effective siRNA/drug codelivery carrier offers great promise to cancer treatment on account of the synergistic effect provided from cancer-associated genes and anticancer drugs (8,25,28,39,47,57). Ever since the discovery of RNA interference (RNAi) (21), gene-specific inhibition has been proposed in cancer treatment to overcome multiple drug resistance and to inhibit expression of upregulated oncogenes that result in unregulated tumor growth (12,13,20,24,31,46). In fact, RNAi-based treatments are regarded as a new class of

Innovation

Controlled codelivery of gene and drugs using carriers for enhanced therapeutic treatment has been a challenging research topic. In the present study, we developed a siRNA/drug codelivery system based on functional mesoporous silica nanoparticles for redox-controlled release. We successfully demonstrated that the nanoparticle carrier could deliver B-cell lymphoma 2 siRNA and doxorubicin both *in vitro* and *in vivo*, leading to enhanced therapeutic efficacy.

[1]Division of Chemistry and Biological Chemistry, School of Physical and Mathematical Sciences, and [2]School of Materials Science and Engineering, Nanyang Technological University, Singapore, Singapore.
[3]Institute of Molecular and Cell Biology, Singapore, Singapore.
[4]Department of Biological Sciences, National University of Singapore, Singapore, Singapore.

therapeutics for human diseases, including cancer. A hurdle to widespread use of free siRNA-based therapeutics is their inefficient intracellular uptake (1,10). The use of non-viral siRNA-based carriers is an attractive strategy for RNAi therapeutics. Issues, including how to enhance the efficiency of cellular uptake and how to carry out the controlled release of siRNA from carriers, need to be addressed in the design of such technology. Both criteria are essential for effective targeted gene silencing to be achieved *in vivo* (34). Such non-viral-based drug carriers can be concomitantly used to improve the delivery of pharmacological anticancer drugs into cancer cells, thereby minimizing undesirable side effects of such drugs.

We selected functional mesoporous silica nanoparticles (MSNPs) as the carrier for codelivery of siRNA and anticancer drug. The unique properties of MSNPs, such as tunable nanoparticle size, uniform mesopore, porous interior amendable to drug loading, high surface area, and easy surface functionalization (17,22,23,26,48), make them highly suitable as a therapeutic delivery vehicle. Previous studies on biological applications of MSNPs have demonstrated their potentials for RNA or drug delivery (2,3,5,33,35,42,50,53,56,58). We here would like to employ multifunctional MSNPs as the carrier for effective codelivery of siRNA and drug in a controlled-release manner. Such desirable traits will minimize adverse side effects resulted from uncontrolled release of both siRNA and drugs.

The work presented here verified the efficacy of siRNA/drug codelivery system based on multifunctional MSNPs, where the mesopores of the nanoparticles are capped by redox-responsive nano-gates, that is, ethylenediamine-modified β-cyclodextrin (CD-2NH_2) rings. Intracellular delivery efficacy was first evaluated in HeLa cells, where siRNA against B-cell lymphoma 2 (*Bcl-2*) was employed. *Bcl-2* was targeted since this protein promotes the tumor formation by preventing cellular apoptosis (7) and contributes to the resistance to anticancer drugs (6,52). This codelivery approach leads to increased apoptosis of HeLa cells treated with CD-2NH_2-capped MSNPs containing *Bcl-2* siRNA and doxorubicin (Dox). Further proof of the delivery principle was achieved in transgenic zebrafish larvae expressing the green fluorescence protein (GFP) reporter in the choroid plexus (16). Here, siRNA/CD-2NH_2-capped MSNPs were injected into brain to cause a reduction of GFP expression. Choroid plexus growth was significantly inhibited in transgenic larvae when treated with high concentration of Dox-loaded CD-2NH_2-capped MSNPs. The anticancer efficacy of the delivery system was further confirmed in a liver tumor model using transgenic zebrafish that express oncogenic EGFP-kras^{v12} (45). This work validated the use of transgenic zebrafish larvae as a well-controlled reporter system to develop the formulations of siRNA/drug complexes and to identify those with the highest *in vivo* potency.

Results and Discussion

To develop a viable carrier for controlled siRNA/drug codelivery, we used functional MSNPs, where the mesopores of the nanoparticles are capped by redox-responsive nanogates, that is, CD-2NH_2 rings (49). As shown in Scheme 1, the disulfide bond-containing amino groups were initially attached to the MSNP surface. The adamantane (AD) units were then introduced onto the surface through the amidation between the amino groups and adamantane-1-carboxylic acid (AD-COOH). Then, the AD units on the nanoparticle surface formed stable host–guest complexes with CD-2NH_2 under the association constant of 10^4–$10^5\ M^{-1}$ (9). In addition to capping drug molecules inside the mesopores, the second role of CD-2NH_2 is to bind siRNA through electrostatic interactions. The mechanism of controlled siRNA/drug release within cancer cells can be realized by the cleavage of redox-responsive disulfide bonds triggered by intracellular glutathione (GSH) (18,27,41,54), leading to the uncapping of the β-CD rings followed by the drug release from the mesopores. siRNA can also be dissociated from CD-2NH_2 on account of intracellular acidic pH, thereby achieving high RNAi at the level required for gene knockdown.

Thiol group-containing MSNPs (MSNP-SH) were prepared through the cocondensation reaction (4,38) of tetraethylorthosilicate (TEOS) and 3-mercaptopyltrimethoxysilane (MPTMS) followed by the removal of structure-directing agent cetyltrimethylammonium bromide (CTAB). The MSNP-SH was characterized by powder X-ray diffraction (XRD) and N_2 adsorption/desorption measurements to confirm the mesoporous structure. In the powder XRD pattern (Supplementary Fig. S1; Supplementary Data are available online at www.liebertpub.com/ars), the sharp peak at $2\theta = 2.12$, corresponding to (100) plane, along with two minor peaks at $2\theta = 3.96$ and $2\theta = 4.60$ for (110) and (200) planes, respectively, clearly prove the hexagonal structure of MCM-41 type MSNPs (30). In addition, a typical type-IV isotherm was obtained, indicating that the MSNP-SH possesses a high Brunauer–Emmett–Teller (BET) surface area of $730\ m^2 \cdot g^{-1}$ and a narrow Barrett–Joyner–Halenda pore size distribution with an average pore diameter of 2.7 nm.

The surface of MSNP-SH was further treated with *S*-(2-aminoethylthio)-2-thiopyridine hydrochloride (SATH) for the formation of the disulfide bonds, leading to amino group-terminated nanoparticles (MSNP-SS-NH_2). AD-functionalized MSNPs (MSNP-SS-AD) were finally prepared by the amidation between MSNP-SS-NH_2 and AD-COOH in the presence of dicyclohexylcarbodiimide (DCC) in dimethylformamide (DMF). The morphology of the MSNP-SH nanoparticles were characterized by field emission scanning electron microscopy (FESEM) (Fig. 1a) and transmission electron microscopy (TEM) (Fig. 1b), showing uniform nanoparticle size with a mean diameter of 150 nm and well-ordered mesoporous structure with the pore diameter of 2–3 nm. The surface modifications of MSNPs were determined by the Fourier transform infrared spectroscopy (FT-IR) analysis (Fig. 1c). After converting thiol groups into the disulfide bond-bridged amino groups on the nanoparticle surface, a minor peak at $2560\ cm^{-1}$ corresponding to the thiol group (36) disappeared, while a new peak observed at $1530\ cm^{-1}$ is assigned to the primary amine. After the amidation for the formation of MSNP-SS-AD, the peak of the amino group centered at $1530\ cm^{-1}$ disappeared. Signals for the AD units on the nanoparticle surface cannot be well identified, since they overlapped with the broad peak from 1100 to $1300\ cm^{-1}$. The BET surface area of MSNP-SS-AD was measured to be $620\ m^2 \cdot g^{-1}$, which is slightly lower than that of MSNP-SH. MSNP-SS-AD was further characterized by solid-state ^{13}C cross polarization and magic angle spinning nuclear magnetic resonance (CP MAS NMR) spectroscopy. The ^{13}C CP MAS NMR spectrum

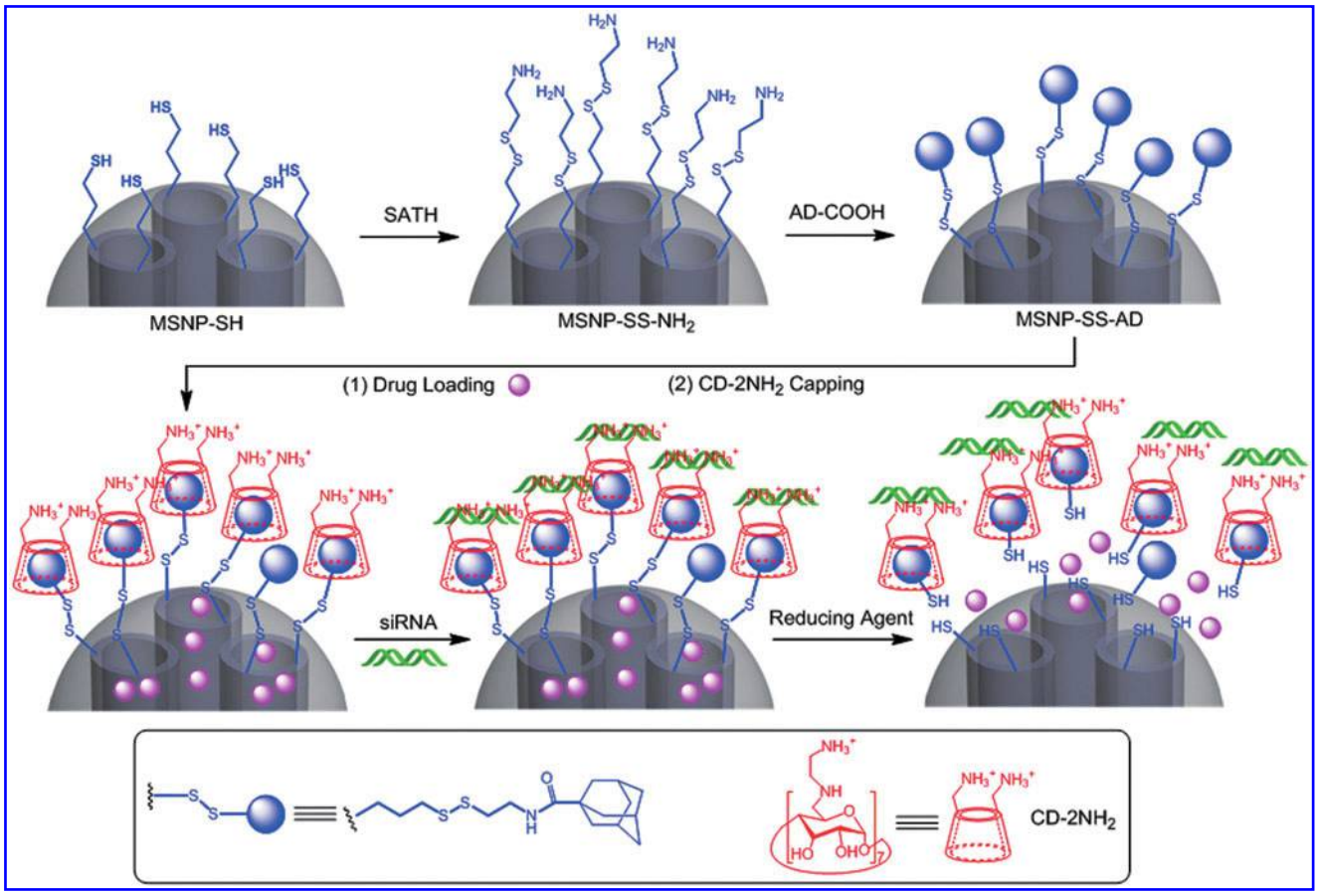

SCHEME 1. Schematic representation of MSNP based siRNA/drug codelivery system. MSNP, mesoporous silica nanoparticle. To see this illustration in color, the reader is referred to the web version of this article at www.liebertpub.com/ars

(Fig. 1d) of MSNP-SS-AD exhibits strong signals at 11.3, 23, 28, 49.5, and 51.5 ppm, which are attributed to the aliphatic secondary carbon atoms. Signals ranging from 34 to 41 ppm in the spectrum are ascribed to the carbon atoms of the AD units, and the signal at 174 ppm is assigned to the carbonyl carbon of the newly formed amide bond. These observations indicate successful preparation of AD-functionalized nanoparticles (MSNP-SS-AD).

Moreover, zeta potential measurements further support the successful surface functionalization of MSNPs (Supplementary Table S1). A negative zeta potential of −24.4 mV for MSNP-SH was converted to a positive value of 22.5 mV for MSNP-SS-NH_2, which can be attributed to the positively charged ammonium species on the surface of MSNP-SS-NH_2. After the introduction of the neutral AD units on the surface, a zeta potential decrease from 22.5 to 12.7 mV was observed in the case of MSNP-SS-AD. The zeta potential measurements also provide clear evidence for the formation of the host–guest complex between AD and CD-2NH_2 on the nanoparticle surface. When MSNP-SS-AD was capped with β-CD through the complexation, the surface charge of the nanoparticles was reversed from a positive value of 12.7 mV to a negative one of −26.7 mV, on account of the presence of the hydroxyl groups from β-CD. However, when CD-2NH_2 was used to cap the nanoparticles, a highly positive surface charge of 19.7 mV was observed because of the protonated amino groups of CD-2NH_2. A positive value of 22.2 mV was observed when MSNP-SS-AD was loaded with Dox followed by the capping of CD-2NH_2, indicating that the presence of Dox inside the mesopores of the nanoparticles would not affect the complex formation. Highly positive surface charge provided by CD-2NH_2 can be employed to bind with negatively charged siRNA through electrostatic interactions, so that the CD-2NH_2-capped MSNP-SS-AD nanoparticles serve as an excellent carrier for the siRNA/drug codelivery. In addition, the introduction of CD-2NH_2 onto the MSNP-SS-AD surface enhances the stability of the nanoparticles in both distilled H_2O and Dulbecco's modified Eagle's medium (DMEM) (Supplementary Fig. S2 and Supplementary Table S2). The average diameter of the nanoparticles in DMEM was significantly decreased as compared with that in H_2O, suggesting increased dispersibility and stability in cell culture medium. Thus, the surface coverage of CD-2NH_2 on MSNP-SS-AD plays a crucial role in cellular internalization, which is an essential step for intracellular siRNA/drug codelivery of using the nanoparticles.

To prove that the drug release was controlled by redox-responsive nano-gates provided by the CD rings, β-CD without any modification was used to complex with MSNP-SS-AD for capping the mesopores. Rhodamine B (RhB) was employed as a model drug, and the loading capacity of MSNP-SS-AD toward RhB was calculated to be 41 μg of RhB per 1 mg of nanoparticles (4.1 wt%), by comparing ultraviolet-visible (UV-vis) absorption intensities of RhB solution before

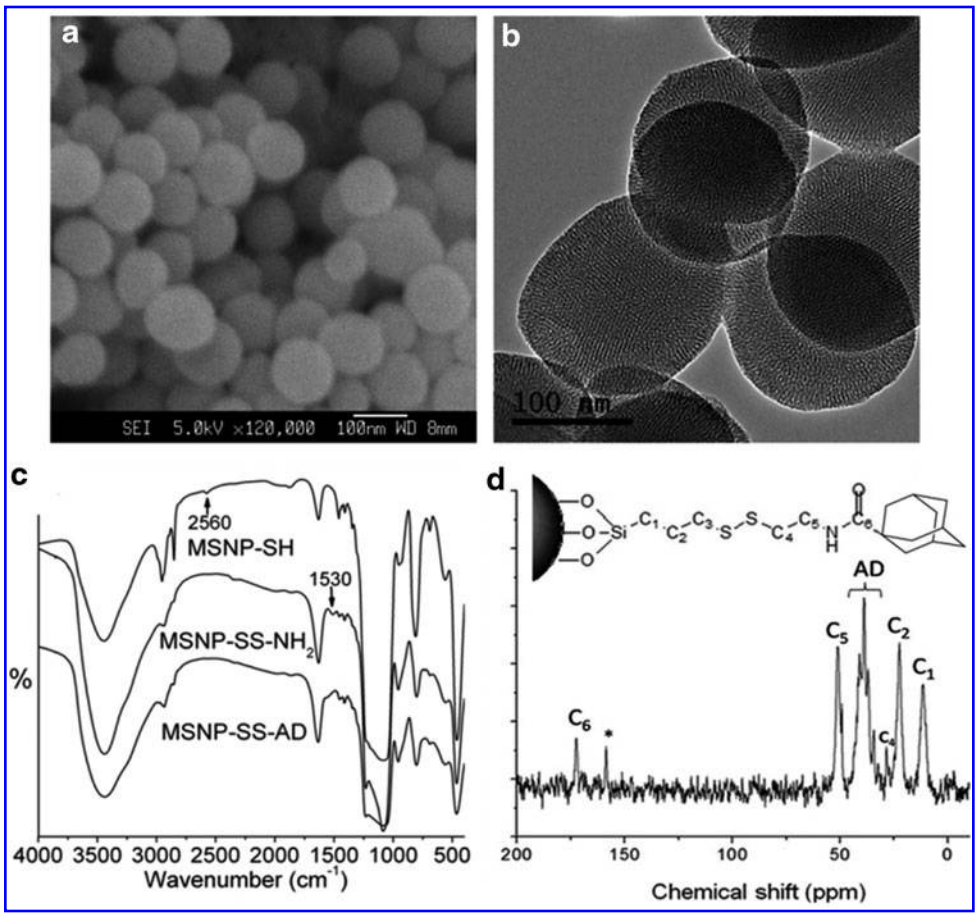

FIG. 1. Characterization figures and spectra of functional MSNP. (a) Field emission scanning electron microscopy and **(b)** transmission electron microscopy images of MSNP-SH; **(c)** FT-IR spectra of MSNP-SH, MSNP-SS-NH_2, and MSNP-SS-AD with different surface modifications; and **(d)** ^{13}C cross polarization and magic angle spinning nuclear magnetic resonance spectrum of MSNP-SS-AD. FT-IR, Fourier transform infrared spectroscopy; MSNP, mesoporous silica nanoparticle; AD, adamantane.

and after adding MSNP-SS-AD. As seen from Figure 2a and b, the leakage of RhB from β-CD-capped MSNP-SS-AD in the absence of reducing agent was negligible, whereas a significant release profile of RhB from β-CD-capped MSNP-SS-AD was observed upon the addition of reducing agent dithiothreitol (DTT). The observation can be explained by pre-installed disulfide bond cleavage on the nanoparticle surface induced by DTT. This cleavage resulted in the dissociation of the β-CD ring, which in turn led to the release of previously loaded RhB. In comparison, the CD-2NH_2-capped MSNP-SS-AD exhibits slower RhB release after the addition of DTT, which may be attributed to stronger blockage caused by the amino group-containing β-CD ring. Similarly, the RhB release profiles in the presence of GSH (25 m*M*) can also be observed. To understand the release mechanism of real anticancer drugs, similar experiments were carried out using Dox-loaded MSNP-SS-AD capped with CD-2NH_2. The loading capacity of MSNP-SS-AD for Dox was 25 μg of Dox per 1 mg of nanoparticles (2.5 wt%). Similar redox-controlled Dox release profiles (Fig. 2c) were observed under the same experimental conditions. To better simulate the Dox release profile in acidic intracellular environment, we conducted the Dox release experiment from Dox-loaded CD-2NH_2-capped MSNP-SS-AD complexed with siRNA (MSNP-SS-AD + Dox + CD-2NH_2-SiRNA complex) under acidic pH condition in DMEM cell culture medium. The results show that the release rate was decreased in acidic environment (Supplementary Fig. S3). A possible reason for the rate decrease might be attributed to stronger electrostatic interaction between siRNA and amine groups of CD-2NH_2 under acidic condition, decreasing the interaction between the reducing agent (DTT or GSH) and embedded disulfide bonds. In fact, redox-controlled release process could even be monitored by naked eye (Supplementary Fig. S4). A sample of RhB loaded MSNP-SS-AD capped with β-CD was placed at the bottom of a fluorescence cuvette containing phosphate buffered saline (PBS) buffer (3 ml, pH 7.4). After the sample was stabilized for 1 h, 50 m*M* DTT was added into the solution. Obvious RhB release in red was observed at the bottom of the cuvette after 5 min.

An essential prerequisite in the design of siRNA delivery vehicle is the ability to form stable complexes with free siRNA. In the case of CD-2NH_2-capped MSNP-SS-AD, the complex formation is mediated by electrostatic interaction between negatively charged siRNA and positively charged amino groups of CD-2NH_2 on MSNP-SS-AD. The electrostatic interaction was demonstrated by the retarded siRNA band mobility in agarose gel electrophoresis, a phenomenon that was not observed with free siRNA. *Bcl-2* siRNA was used in this electrophoresis experiment. As shown in Figure 2d, free siRNA in the first lane has the highest mobility. Upon increasing the nanoparticle-to-siRNA weight ratios (lanes 3–8, Fig. 2d), a gradual decrease in the band mobility and intensity was observed. siRNA concentration was kept constant in all lanes, except in lane 2, where no siRNA was loaded. siRNA became fully condensed on the nanoparticle surface when the nanoparticle-to-siRNA weight ratio reached 110:1. When DTT (50 m*M*) was added into a sample with a nanoparticle-to-siRNA weight ratio of 110:1 (last lane, Fig. 2d), the recovery of

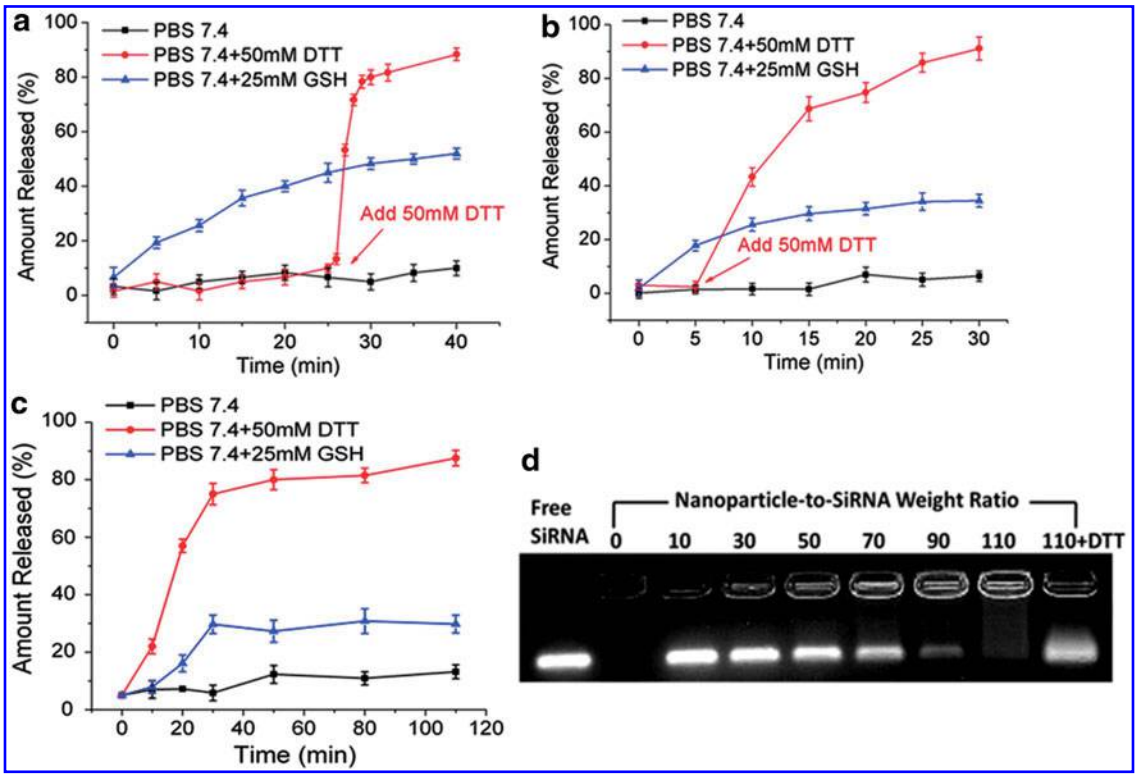

FIG. 2. Redox-controlled drug/siRNA release from functional MSNP. Controlled drug release profiles in PBS (pH = 7.4) for **(a)** RhB release from *β*-CD-capped MSNP-SS-AD, **(b)** RhB release from CD-$2NH_2$-capped MSNP-SS-AD, and **(c)** Dox release from CD-$2NH_2$-capped MSNP-SS-AD. **(d)** Agarose gel electrophoresis of the siRNA complexation with CD-$2NH_2$-capped MSNP-SS-AD under different nanoparticle-to-siRNA weight ratios. Lanes from *left* to *right* are free siRNA, CD-$2NH_2$-capped MSNP-SS-AD, and CD-$2NH_2$-capped MSNP-SS-AD/siRNA complexes under the nanoparticle-to-siRNA weight ratios of 10:1, 30:1, 50:1, 70:1, 90:1, 110:1, and 110:1 containing 50 m*M* DTT, respectively. PBS, phosphate buffered saline; RhB, rhodamine B; CD, cyclodextrin; DTT, dithiothreitol. To see this illustration in color, the reader is referred to the web version of this article at www.liebertpub.com/ars

siRNA band intensity was detected. This result demonstrates that attached siRNA can be released from the nanoparticle surface by redox-triggered disulfide bond cleavage. GSH (25 m*M*) can also be used to induce the disulfide bond cleavage on the nanoparticle surface, releasing both drug and siRNA for synergistic chemotherapeutic therapy.

To trace the location of the nanoparticles in cells, green fluorescent fluorescein isothiocyanate (FITC) was embedded inside the silica nanoparticles during the fabrication process. Cellular uptake of FITC-labeled MSNP-SS-AD loaded with Dox and capped with CD-$2NH_2$ (MSNP-SS-AD(FITC) + Dox + CD-$2NH_2$) was investigated by confocal laser scanning microscopy (CLSM) using HeLa cells as the cancer cell model. The nuclei in HeLa cells were stained blue by 4′,6-diamidino-2-phenylindole (DAPI). Green fluorescence (Fig. 3e) was detected around the cell nucleus, indicating effective nanoparticle internalization by HeLa cells. No green fluorescence was detected outside the cancer cells. In comparison, less green fluorescence was detected in HeLa cells, when cellular uptake of FITC-labeled MSNP-SS-AD was assessed (Supplementary Fig. S5). Hence, FITC-labeled MSNP-SS-AD capped with CD-$2NH_2$ presents much higher cellular internalization capacity, confirming its potential for intracellular therapy. Flow cytometry analysis also supports the enhancement of cellular uptake by the CD-$2NH_2$ capping (Supplementary Fig. S5g). The CLSM image demonstrated successful release of Dox from MSNP-SS-AD within HeLa cells induced by endogenous GSH (Fig. 3d–i), as shown by the presence of red fluorescent Dox in both cytosol and nucleus. Comparison of the fluorescence intensity reading from FITC and Dox inside HeLa cells further proves the Dox release from the nanoparticles (Supplementary Fig. S6). These observations indicate effective redox-triggered intracellular release of Dox from the nanoparticles and successful delivery of Dox into the nucleus, where the anticancer activity of Dox is executed by its interactions with DNA (15). In addition, the detection of FITC-labeled and CD-$2NH_2$-capped MSNP-SS-AD containing *Bcl-2* siRNA/Dox in perinuclear regions of cytoplasm suggests that the codelivery carrier could bypass the efflux pump resistance observed in HeLa cells (19,55), thereby enhancing Dox-mediated cytotoxicity. Thus, Dox delivered by CD-$2NH_2$-capped MSNP-SS-AD is protected from the degradation by extracellular enzymes, exhibiting enhanced cellular uptake in cancer cells (44).

Moreover, we conducted time-dependent CLSM experiments on HeLa cells treated with MSNP-SS-AD(FITC) + Dox + CD-$2NH_2$ and equivalent amount of free Dox (Supplementary Fig. S7). Free Dox can quickly diffuse into cell nucleus and reach the equilibrium within 2 h, as no further enhancement of the Dox fluorescence was observed after 2 h. On the contrary, for Dox delivered by the MSNP carrier, sustained Dox release inside HeLa cells was observed, indicated by the increasing Dox fluorescence intensity inside the cell nucleus and cytoplasm. The sustained Dox release from

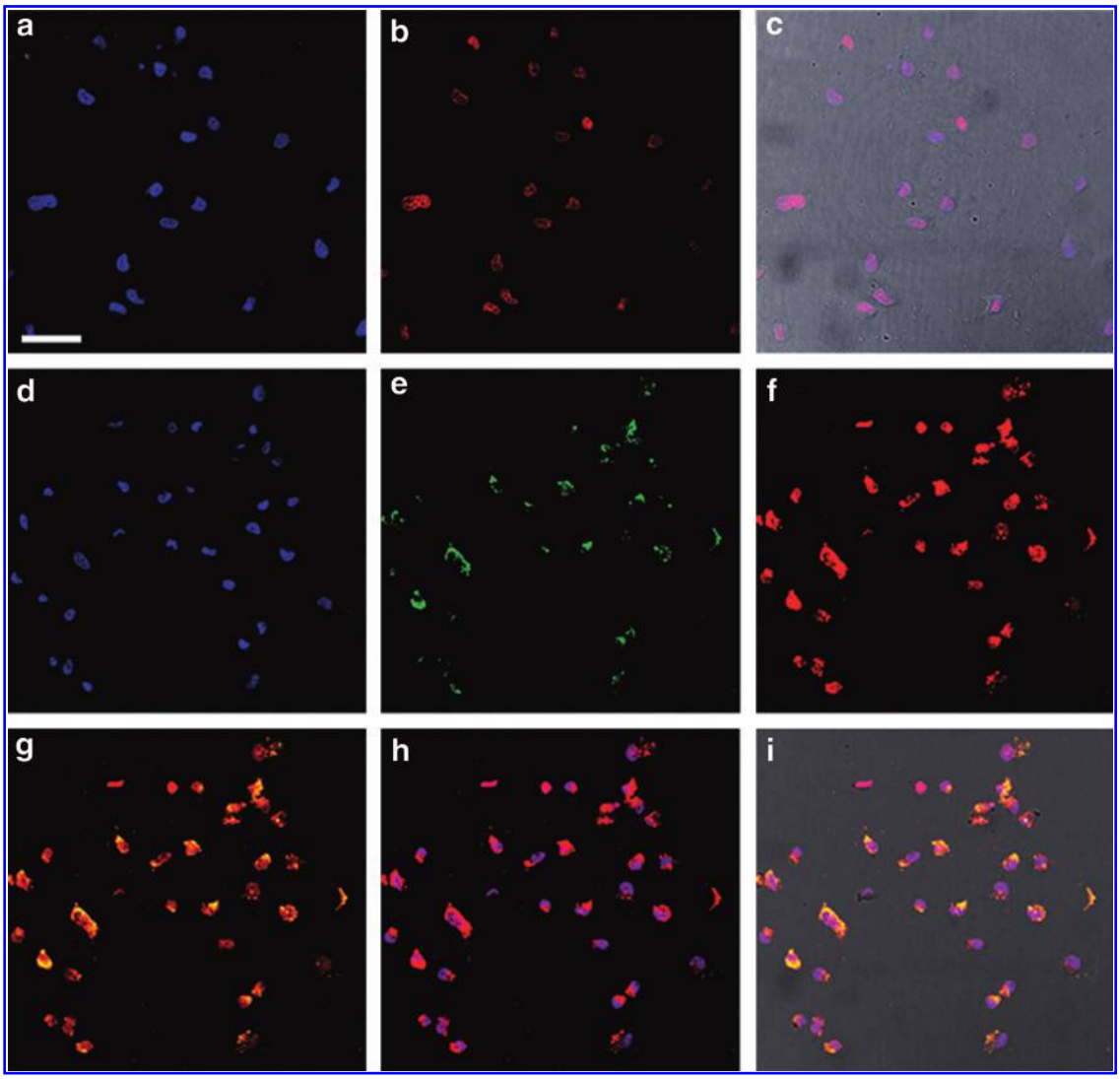

FIG. 3. Cellular internalization of functional MSNP and intracellular Dox release. Confocal laser scanning microscopy images of HeLa cells treated with **(a–c)** equivalent amount of free Dox and **(d–i)** FITC-labeled CD-2NH$_2$-capped MSNP-SS-AD loaded with Dox (50 $\mu g \cdot ml^{-1}$) for 24 h. **(a)** Blue fluorescence from DAPI, **(b)** red fluorescence from Dox, **(c)** overlay of bright field from images **(a)** and **(b)**; **(d)** blue fluorescence from DAPI, **(e)** green fluorescence from FITC-labeled MSNP-SS-AD, **(f)** red fluorescence from released Dox, **(g)** overlay of images **(e)** and **(f)**, **(h)** overlay of images **(d)** and **(f)**, and **(i)** overlay of bright field from images **(d–f)**. Dox, doxorubicin; FITC, fluorescein isothiocyanate; DAPI, 4′,6-diamidino-2-phenylindole. To see this illustration in color, the reader is referred to the web version of this article at www.liebertpub.com/ars

the MSNP carrier could enhance the chemotherapy effect by maintaining effective cancer-killing dosage for a relatively long time. Then, we carried out experiments to assess the amounts of MSNP-SS-AD(FITC) and Dox inside HeLa cells after treated with MSNP-SS-AD(FITC) + Dox + CD-2NH$_2$ + siRNA (25 and 50 $\mu g \cdot ml^{-1}$, respectively) for 24 h. After the treatment, the HeLa cells were washed with PBS three times and then collected by trypsin. The cell density was determined by using cell-counting plate. The cells were treated with lysis buffer to break the cell membrane and the mixture solution was suspended in deionized H_2O (1 ml) for fluorescence measurement. The amounts of MSNP-SS-AD(FITC) and Dox were quantified by the fluorescence intensity of FITC and Dox, respectively. MSNP-SS-AD(FITC) and Dox solutions with known concentrations were used as standard references for the quantification. The results (Supplementary Fig. S8) indicate that the amounts of MSNP-SS-AD(FITC) and Dox in the cells were ca. 5 μg and 61 ng per 10^6 cells when 25 $\mu g \cdot ml^{-1}$ of MSNP-SS-AD(FITC) + Dox + CD-2NH$_2$ + siRNA was used, and ca. 17 μg and 210 ng per 10^6 cells when 50 $\mu g \cdot ml^{-1}$ of MSNP-SS-AD(FITC) + Dox + CD-2NH$_2$ + siRNA was used.

To assess the efficacy of gene knockdown mediated by *Bcl-2* siRNA delivered by CD-2NH$_2$-capped MSNP-SS-AD, the level of *Bcl-2* protein expression in transfected HeLa cells was evaluated by western blot. After disrupting the cell membrane with lysis buffer, the protein concentration of each sample was quantified by Pierce® BCA Protein Assay Kit. Protein concentration of all the six samples was around 1000 $\mu g \cdot ml^{-1}$ (Supplementary Fig. S9). No obvious cell death was detected in HeLa cells transfected with CD-2NH$_2$-capped MSNP-SS-AD alone, CD-2NH$_2$-capped MSNP-SS-AD/*Bcl-2* siRNA complex, or free siRNA. Commercially available Lipofectamine®

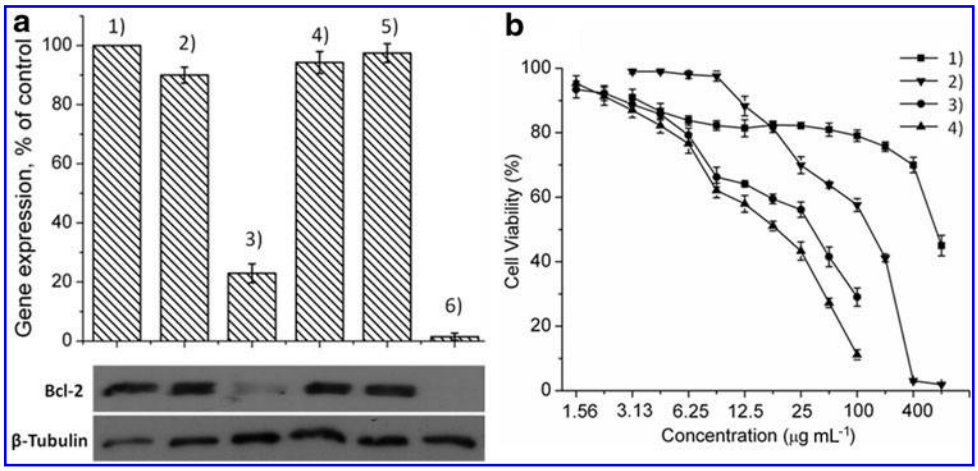

FIG. 4. ***Bcl-2* protein silence and enhanced chemotherapy effect. (a)** *Bcl-2* protein knockdown by CD-2NH_2-capped MSNP-SS-AD/siRNA(+) complex (MSNP-SS-AD + CD-2NH_2 + siRNA) in HeLa cells (nanoparticle-to-siRNA weight ratio of 110:1). Gene expression was evaluated by the ratio of intensity of the *Bcl-2* band to that of the internal standard, *β*-tubulin. The ratio of each sample was normalized to the value of the sample without any treatment. **(a-1)** control, **(a-2)** MSNP-SS-AD + CD-2NH_2, **(a-3)** MSNP-SS-AD + CD-2NH_2 + siRNA(+), **(a-4)** MSNP-SS-AD + CD-2NH_2 + siRNA(−), **(a-5)** free siRNA, and **(a-6)** Lipofectamine + siRNA(+). **(b)** Relative cell viability of HeLa cells treated with indicated samples under an equivalent amount of nanoparticle concentration and equivalent amount of Dox. **(b-1)** MSNP-SS-AD + CD-2NH_2 + siRNA(−), **(b-2)** free Dox, **(b-3)** MSNP-SS-AD + Dox + CD-2NH_2, and **(b-4)** MSNP-SS-AD + Dox + CD-2NH_2 + siRNA(+). Nanoparticle-to-siRNA weight ratio is 100:1. *Bcl-2*, B-cell lymphoma 2.

RNAiMAX reagent (Invitrogen) was used as a positive siRNA delivery control [siRNA(+)]. Non-binding siRNA duplex was used as a negative control [siRNA(−)] to exclude non-specific cytotoxic effect of siRNA. Protein expression results show that *Bcl-2* protein was not detected in cells transfected with the Lipofectamine RNAiMAX reagent, confirming the silencing efficacy of the chosen siRNA(+) sequence against *Bcl-2* protein (Fig. 4a, lane 6). Transfection of cells with CD-2NH_2-capped MSNP-SS-AD/*Bcl-2* siRNA complex resulted in 70% reduction of *Bcl-2* protein expression (lane 3). Delivery of CD-2NH_2-capped MSNP-SS-AD alone (lane 2) did not interfere the expression of endogenous *Bcl-2* protein. These observations indicate that no obvious cytotoxicity was associated with the siRNA carrier and that the protein silencing observed in transfected HeLa cells was attributed to siRNA(+) electrostatically associated with the surface of nanoparticles. No *Bcl-2* protein knockdown was detected in cells transfected with CD-2NH_2-capped MSNP-SS-AD/siRNA(−) complex (lane 4), where siRNA(−) was represented by the non-binding siRNA duplex. Free siRNA alone also failed to decrease the expression of endogenous *Bcl-2* protein (lane 5). Thus, the transfection studies in HeLa cells demonstrate the efficacy of CD-2NH_2-capped MSNP-SS-AD as an siRNA carrier to mediate intracellular silencing of expression of targeted protein.

Synergistic anticancer effect caused by simultaneous delivery of anticancer drug Dox and *Bcl-2* siRNA was investigated using the 3-(4,5-dimethylthiazol-2-yl)-2,5-diphenyltetrazolium bromide (MTT) cytotoxicity assay. The bar chart in Figure 4b shows that CD-2NH_2-capped MSNP-SS-AD/siRNA complex exhibits little cytotoxic effect, since relative cell viability in transfected cells remains about 80% until extremely high nanoparticle dose is used (Fig. 4b-1). Its IC50 (concentration killing 50% cells) value was determined to be 600 $\mu g \cdot ml^{-1}$. A significant increase in cytotoxicity was detected in HeLa cells exposed to Dox-loaded and CD-2NH_2-capped MSNP-SS-AD (Fig. 4b-3), when compared to the exposure with equivalent amount of free Dox (Fig. 4b-2). The results further confirm enhanced cellular uptake and intracellular redox-triggered release of Dox from CD-2NH_2-capped MSNP-SS-AD carrier, agreeing well with previous reports using MSNPs as drug carriers (5,42). The IC50 value of Dox-loaded CD-2NH_2-capped MSNP-SS-AD is 37.2 $\mu g \cdot ml^{-1}$. Simultaneous delivery of Dox and *Bcl-2* siRNA [siRNA(+)] further enhances the cytotoxic effect, as overall cell viability further decreased and its IC50 value was determined to be 17.5 $\mu g \cdot ml^{-1}$ (Fig. 4b-4). To further demonstrate that the enhanced chemotherapy is due to *Bcl-2* protein silence, we carried out some control experiments. While silencing the *Bcl-2* protein expression by using CD-2NH_2-capped MSNP-SS-AD/*Bcl-2* siRNA complex, free Dox was also added (Supplementary Fig. S10b-2). Compared to the sample only treated with free Dox (Supplementary Fig. S10b-3), lower cell viability was observed with this approach. However, the cell viability is still higher than that when Dox was delivered by the nanoparticles (Supplementary Fig. S10a-2, a-5), which confirms the enhanced drug uptake by using the nanoparticle-based delivery system. Thus, CD-2NH_2-capped MSNP-SS-AD presents itself as a multifunctional carrier with enhanced chemotherapeutic efficacy mediated by improved cellular uptake and codelivery of drug/siRNA.

In vivo chemotherapeutic efficacy of CD-2NH_2-capped MSNP-SS-AD was further analyzed in transgenic zebrafish larvae (Supplementary Fig. S11). Zebrafish share several comparable tissues, organs, and glands with mammals, which can develop into diseases resembling human disorders. The transparent zebrafish larvae with their comparatively short development cycle *ex-utero* could serve as an attractive and rapid system for validating novel therapeutic agents (43). Externally developing zebrafish larvae are amendable to microsurgical manipulations. Bioimaging of tissues expressing a fluorescent protein reporter can be easily achieved with a standard CLSM due to optical translucence of the relatively

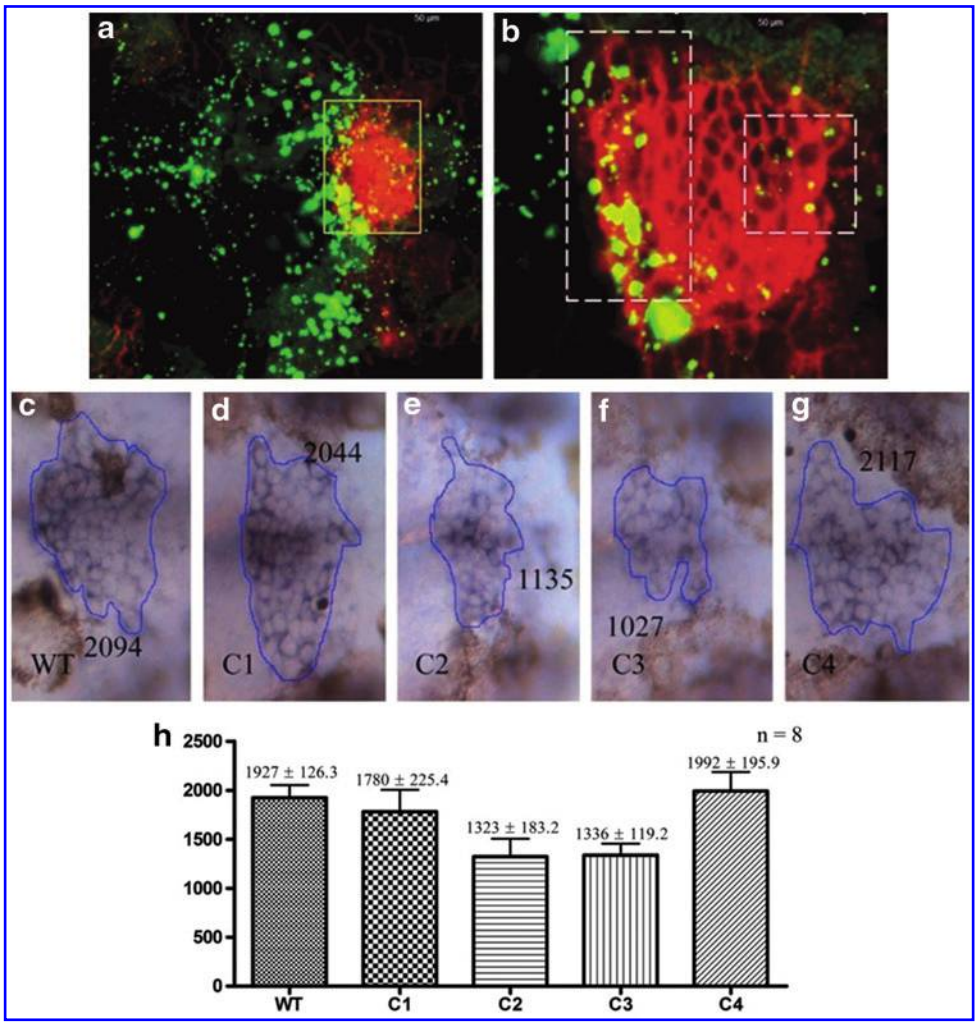

FIG. 5. ***In vivo*** **uptake of CD-2NH$_2$-capped MSNP-SS-AD inhibits transcription of GFP in the epithelial cells of choroid plexus at the 4th ventricle of zebrafish larval brain. (a, b)** Brain-targeted delivery of FITC labeled CD-2NH$_2$-capped MSNP-SS-AD resulted in uptake into some cells largely in peripheral areas of the choroid plexus, highlighted by boxes. **(c–g)** Specific weight ratios of CD-2NH$_2$-capped MSNP-SS-AD/GFP siRNA complexes (C2 and C3) enhance inhibition of GFP transcription *in vivo*. The area (μm^2) of GFP expression detected by whole mount *in situ* hybridization in the choroid plexus is quantified by the Image J software. **(h)** The average size of the choroid plexus is presented in a bar chart with values shown as mean ± standard error of mean. Formulations for various weight ratios of CD-2NH$_2$-capped MSNP-SS-AD nanoparticle/siRNA complexes used for this experiment are as follows: WT (without any treatment), C1 (0.04 $\mu g \cdot \mu l^{-1}$ siRNA only), C2 (0.12 $\mu g \cdot \mu l^{-1}$ nanoparticle with 0.04 $\mu g \cdot \mu l^{-1}$ siRNA, 3:1), C3 (0.2 $\mu g \cdot \mu l^{-1}$ nanoparticle with 0.04 $\mu g \cdot \mu l^{-1}$ siRNA, 5:1), and C4 (0.4 $\mu g \cdot \mu l^{-1}$ nanoparticle with 0.04 $\mu g \cdot \mu l^{-1}$ siRNA, 10:1). GFP, green fluorescence protein. To see this illustration in color, the reader is referred to the web version of this article at www.liebertpub.com/ars

small developing larvae, which at 5 days is 4 mm long. Thus, we made use of the similarity in high rate of cellular proliferation during embryonic tissue growth to model unregulated proliferations in cancer cells (37). Since more than 80% of human cancers (such as skin cancer and lung, stomach, and mammary tumors) derive from epithelial tissues (14,40), the choroid plexus, a tissue of epithelial origin, was selected to model primary tumor growth. Two zebrafish transgenic lines with GFP (Et(krt4:EGFP)sqet33e20 or SqET33-e20) and membrane localized with KillerRed (SqKR19) expression in the choroid plexus were chosen as the *in vivo* epithelial tissue models to assess cellular uptake of drugs delivered by the nanoparticles and their impact on choroidal epithelial cell proliferation (Supplementary Fig. S11). Imaging in these optically transparent transgenic larvae provides initial assessment of anti-proliferative therapy mediated by Dox-loaded CD-2NH$_2$-capped MSNP-SS-AD *in vivo*.

We first verified *in vivo* cellular uptake of CD-2NH$_2$-capped MSNP-SS-AD. Passive targeting was conducted by microinjecting 0.4 $\mu g \cdot \mu l^{-1}$ CD-2NH$_2$-capped FITC-labeled MSNP-SS-AD into the brain ventricle of SqKR19 transgenic zebrafish larvae (29) after 36 hours post fertilization (hpf). Being located dorsal to the IV ventricle cavity and immediately under the skin, the choroid plexus is an easily accessible site. The morphology of choroidal epithelial cells was highlighted by membrane-localized KillerRed in SqKR19 transgenics (Fig. 5b). The fluorescent signal of internalized FITC from MSNP-SS-AD was observed inside choroidal epithelial cells 2 days after injection. Cells that internalized FITC-loaded nanoparticles were predominantly found in peripheral regions of

the choroid plexus defined by white serrated boxes (Fig. 5b). Next, the efficiency of *in vivo* anti-GFP siRNA interference was assessed using the SqET33-e20 transgenic zebrafish larvae (16) expressing cytosolic GFP in the choroid plexus. Briefly, GFP-positive choroidal cells were first detected at 28 hpf in the layer of neuroepithelial cells, and at 36 hpf they formed a cellular sheet representing the roof of the IV ventricle. These cells then converged toward the midline to form the button-like choroid plexus represented by two to three layers of cells at 3 days post fertilization (dpf). Microinjection of siRNA-containing CD-2NH_2-capped MSNP-SS-AD into the brain ventricle was conducted at 36 hpf. Injected larvae were grown for 2 days before being processed for analysis of GFP siRNA expression by whole mount *in situ* hybridization (WISH). siRNA duplex targeting EGFP (CAA GCU GAC CCU GAA GUU CTT; IDT) was used for this experiment (Supplementary Fig. S12). To minimize potential off-target effect of GFP siRNA reported in cell lines (51), a standardized low dose of 0.04 $\mu g \cdot \mu l^{-1}$ GFP siRNA was used in all brain ventricle injections to knockdown GFP transcripts in the choroid plexus. The efficacy of GFP knockdown mediated by free GFP siRNA and by the same amount of GFP siRNA complexed with different weight ratios of CD-2NH_2-capped MSNP-SS-AD was compared. Formulations were prepared and incubated over ice for 2 h before the brain ventricle injection. Free GFP siRNA at a concentration of 0.04 $\mu g \cdot \mu l^{-1}$ was inefficient in decreasing GFP transcripts (Fig. 5d). Enhanced GFP knockdown was detected when 3:1 or 5:1 weight ratio of CD-2NH_2-capped MSNP-SS-AD was complexed to 0.04 $\mu g \cdot \mu l^{-1}$ siRNA (Fig. 5e, f), while increasing the weight ratio to 10:1 reversed this trend (Fig. 5g). CD-2NH_2-capped MSNP-SS-AD/GFP siRNA complexes with weight ratios of 3:1 (C2) and 5:1 (C3) inhibit more efficient GFP transcription than that caused by the injection of free GFP siRNA alone (C1). Interestingly, the ability to inhibit GFP transcription was lost when the weight ratio of CD-2NH_2-capped MSNP-SS-AD to GFP siRNA was increased to 10:1 (C4 in Fig. 5h). This observation suggests that excess of positively charged CD-2NH_2-capped MSNP-SS-AD interferes with intracellular release of GFP siRNA, which in turn impedes GFP silencing with inefficient GFP knockdown.

In vivo release of internalized Dox mediated by redox-responsive CD-2NH_2-capped MSNP-SS-AD nanocarrier was then investigated. We performed localized delivery of Dox by the nanoparticles to sites flanking the choroid plexus, to mimic localized delivery of anticancer drugs into the vicinity of tumor cells. The effect of internalized Dox was assessed based on the inhibition of tissue proliferation in choroidal epithelial cells where the Dox-loaded nanoparticles were internalized. Again, transgenic larvae were injected at 36 hpf and the effect on choroid plexus growth and GFP intensity was assessed. Different weight ratios of injected Dox-loaded nanoparticles complexed with GFP siRNA were evaluated. Six transgenic larvae were imaged 2 days post injection for each formulation. Untreated transgenic larvae were used as a control for normal growth of choroid plexus and intensity of GFP expression (Supplementary Figs. S13 and S14). In larva exposed to C3 (0.2 $\mu g \cdot \mu l^{-1}$ Dox-loaded nanoparticles with 0.04 $\mu g \cdot \mu l^{-1}$ siRNA, 5:1) and C4 (0.4 $\mu g \cdot \mu l^{-1}$ Dox-loaded nanoparticles with 0.04 $\mu g \cdot \mu l^{-1}$ siRNA, 10:1) formulations, the shape of the choroid plexus changed and GFP fluorescence was reduced (Supplementary Fig. S13d, e). These changes were noticed upon single injection of the formulation with concentration above 0.2 $\mu g \cdot \mu l^{-1}$ of Dox-loaded CD-2NH_2-capped MSNP-SS-AD. A second set of experiments was conducted in 3-day-old transgenic larvae, where reiterative injections of the same formulation were made into the brain ventricle on two consecutive days. The impact on choroid plexus was then assessed at 7 dpf. When compared to uninjected controls, the injection of free anti-GFP siRNA decreased the mean GFP intensity by 45% (Fig. 6b) without any effect on tissue morphology, that is, the cellular uptake of GFP siRNA had no effect on maintenance of already formed choroid plexus. Injection of increased weight ratio of Dox-loaded CD-2NH_2-capped MSNP-SS-AD/GFP siRNA complex caused defect of the choroid plexus. This phenomenon correlated with the internalization of Dox-loaded carrier and the appearance of clones of GFP-negative choroidal epithelial cells (Fig. 6c, d). The most significant effect was detected upon injection by two consecutive doses of C4 formulations (0.4 $\mu g \cdot \mu l^{-1}$ Dox-loaded CD-2NH_2-capped MSNP-SS-AD with 0.04 $\mu g \cdot \mu l^{-1}$ siRNA, 10:1), the highest concentration of Dox used for this set of experiment. Here, the GFP expression was lost not only in epithelial cells of the midline cluster, but also in glial cells of the choroid plexus located in rhombic lips (*i.e.*, adjacent walls of hindbrain, HB; Fig. 6e). Thus, a positive correlation was observed between disturbed morphology of choroid plexus and the amount of injected Dox-loaded CD-2NH_2-capped MSNP-SS-AD. Although the drug carrier, CD-2NH_2-capped MSNP-SS-AD, was designed for tumor-targeted drug delivery, we compared the tissue distributions of free Dox (250 $\mu g \cdot ml^{-1}$) and Dox-loaded nanoparticles (10 $mg \cdot ml^{-1}$) when they were introduced into systemic circulation by pericardial injection. The dose for this experiment was adjusted 10-fold higher for whole larva detection by CLSM. Transgenic zebrafish that express EGFP in all blood vessels TG(fli1:GFP) was used as the reporter line in this experiment (32). Larva toxicity was detected in the group injected with free Dox. In this group, reduced larval growth and concurrent fluid accumulation in the body (edema) were observed in five out of six injected larvae after 3 days post injection. The developmental defect was only observed in one out of six larvae injected by Dox-loaded nanoparticles (Supplementary Fig. S15). Hence, redox-triggered Dox release by CD-2NH_2-capped MSNP-SS-AD led to lesser side effects than that of free Dox.

We proceeded to verify the anticancer property of Dox-loaded CD-2NH_2-capped MSNP-SS-AD by using a zebrafish mifepristone-inducible liver tumor model that expresses oncogenic EGFP-$kras^{v12}$. Hyperplastic growth of liver tumors was induced in larvae from 4 dpf (45). The advantage of this model is a possibility to visualize and quantify the changes in liver with CLSM. We injected 5 nl of Dox-loaded CD-2NH_2-capped MSNP-SS-AD at a concentration of 10 $mg \cdot ml^{-1}$ into the abdomen of inducible $kras^{v12}$ transgenic zebrafish larvae at 4 dpf. The anticancer property of Dox-loaded nanoparticles was assessed after 6-day post injection using LSM510 META. Representative images of non-injected transgenic larvae (Fig. 7a) and Dox-containing nanoparticle-injected transgenic larvae (Fig. 7b) experiencing liver hyperplasia are presented. All supporting materials that contribute to the bar chart in Figure 7d are shown in Supplementary Figure S16. On average, the liver tumor area was 35.5% less in transgenic larvae that were exposed to Dox-loaded CD-2NH_2-capped MSNP-SS-AD

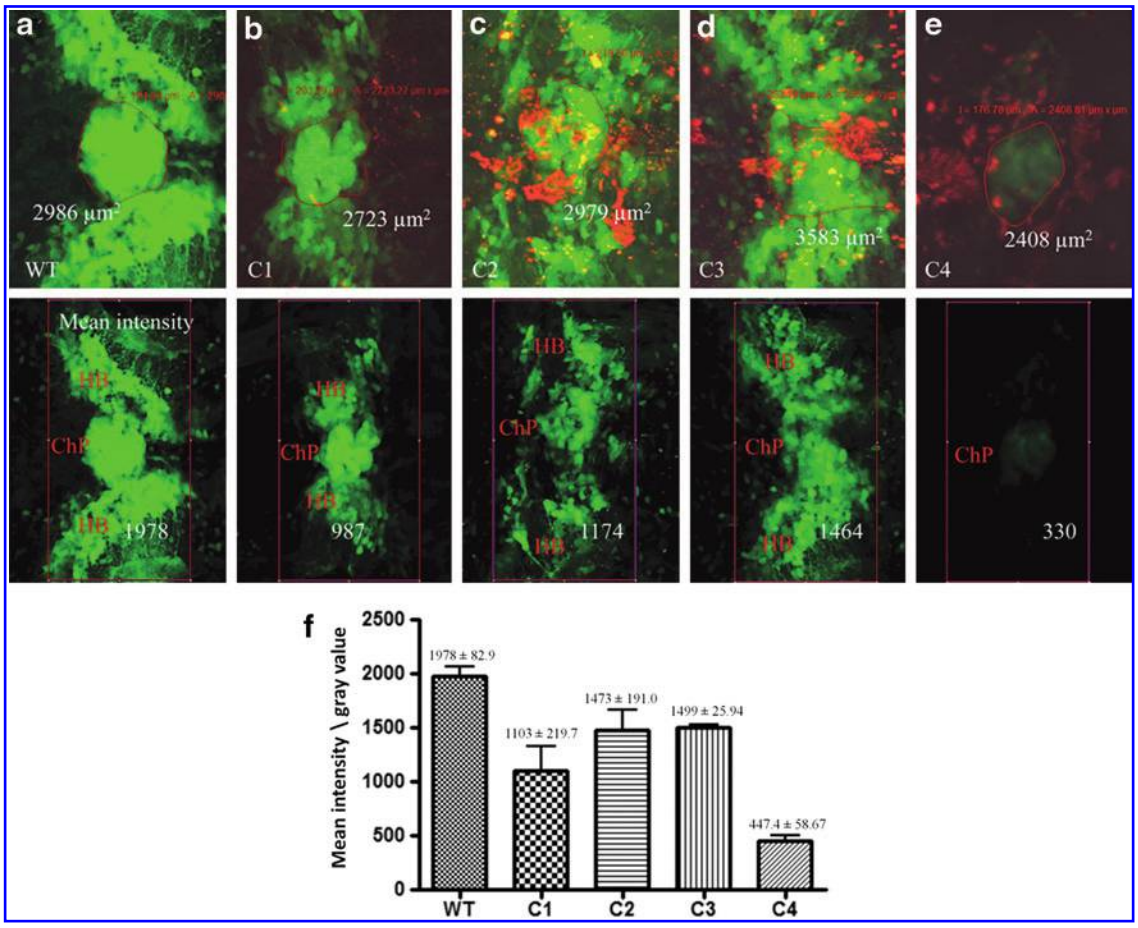

FIG. 6. Significant decrease of GFP expression was observed after two reiterative injections of Dox-loaded CD-2NH$_2$-capped MSNP-SS-AD complexed with GFP siRNA. (a–e) Same weight ratio of Dox-loaded nanoparticle/GFP siRNA complex injected into the brain ventricle on two consecutive days. The impact on GFP expression in the choroid plexus was assessed 2 days later. Barely visible GFP expression in the choroid plexus was detected in all transgenic larvae exposed to the highest weight ratio (C4) of Dox-loaded nanoparticle/GFP siRNA complex. **(f)** The average GFP intensity quantified in the boxed area of the choroid plexus is presented in a bar chart with values stated as mean ± standard error of mean. Values are compiled from three separate injections. The same acquisition setting was used for image capture using LSM510 META confocal microscope. Image intensity was assessed using the Image J software. To see this illustration in color, the reader is referred to the web version of this article at www.liebertpub.com/ars

($n=10$), than that of non-injected transgenic zebrafish experiencing liver hyperplasia ($n=8$). Two-tailed t-test confirmed that the reduction of liver tumor is statistically significant ($P=0.0291$). A magnified view of GFP-positive liver tumor cells with internalized Dox (red fluorescent areas in Fig. 7c) further supports the conclusion that the reduction of hyperplastic liver is due to successful internalization and release of Dox from CD-2NH$_2$-capped MSNP-SS-AD. We also observed significant inhibition of the liver tumor growth after the treatment of Dox-loaded CD-2NH$_2$-capped MSNP-SS-AD (2 and 5 $\mu g \cdot ml^{-1}$, respectively) and *in vivo* Dox release by using the CLSM (Supplementary Fig. S17). The determination of fluorescent intensity of Dox inside the liver tumor provides quantitative indication of the Dox release in the liver tumor.

In conclusion, we have successfully fabricated a redox-responsive drug/siRNA codelivery system based on MSNPs (MSNP-SS-AD). Ethylenediamine-modified β-cyclodextrin (CD-2NH$_2$) rings have been introduced onto the nanoparticle surface as smart nano-gates to (i) block drug molecules within the mesopores and (ii) provide a platform for the complexation with siRNA through electrostatic interactions. Controlled drug/siRNA release from multifunctional nanoparticles by redox-triggered disulfide bond cleavage has been demonstrated in solution. Successful RNAi using siRNA to target two different genes has proved the efficacy of CD-2NH$_2$-capped MSNP-SS-AD as a delivery vehicle for siRNA under a broad range of temperatures. First, the inhibition of *Bcl-2* expression has been detected in *Bcl-2* siRNA transfected HeLa cell lines maintained at 37°C. Second, the *in vivo* experiment carried out in transgenic zebrafish larvae (maintained at 28.5°C) has showed that CD-2NH$_2$-capped MSNP-SS-AD/GFP siRNA complex injected into the brain ventricle decreases GFP transcription in two different populations of cells of the choroid plexus. CD-2NH$_2$-capped MSNP-SS-AD could be used as a carrier for simultaneous anticancer drug (Dox) and siRNA delivery. Enhanced cytotoxicity caused by simultaneous delivery of Dox/*Bcl-2* siRNA has been demonstrated in HeLa cells. Enhanced cytotoxicity has not been observed upon the injection of Dox-loaded nanoparticle/GFP

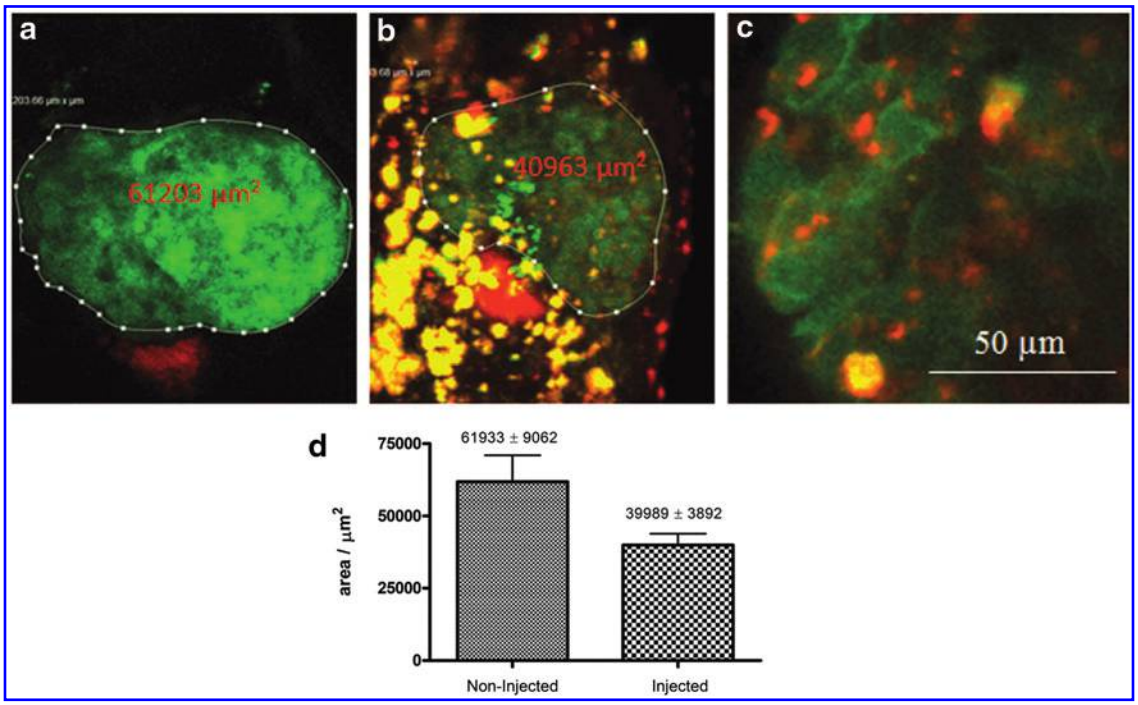

FIG. 7. The liver tumor in the inducible kras^{v12} transgenic zebrafish model was reduced after exposure to Dox-loaded CD-2NH$_2$-capped MSNP-SS-AD when compared with untreated control. (a) A view of transgenic zebrafish larvae Kras^{v12} experiencing liver hyperplasia at 10 days post fertilization. **(b)** A view of transgenic zebrafish larvae experiencing liver hyperplasia after 6 days post injection of Dox-loaded CD-2NH$_2$-capped MSNP-SS-AD. **(c)** A magnified view of liver tumor cells exposed to Dox-loaded CD-2NH$_2$-capped MSNP-SS-AD. Released Dox (red) can be seen inside liver tumor cells colored in green. **(d)** The average area of liver tumor between non-injected control ($n=8$) and siblings injected with Dox-loaded CD-2NH$_2$-capped MSNP-SS-AD ($n=10$) quantified after 6 days post injection is presented as a bar chart with values stated as mean liver area ± standard error of mean. Liver size from each specimen was quantified using the associated software in LSM510 META. To see this illustration in color, the reader is referred to the web version of this article at www.liebertpub.com/ars

siRNA complex since GFP siRNA represents physiologically benign target. In contrast, not only Dox-loaded CD-2NH$_2$-capped MSNP-SS-AD has been internalized by cells *in vivo*, but the development of choroid plexus and the progression of liver hyperplasia have also been inhibited by Dox-loaded nanoparticles in a dose-dependent manner. Lack of inhibition of GFP transcripts by high weight ratio formulations of nanoparticle/siRNA complex (≥10:1) has indicated that the activity of formulations of drug/siRNA needs to be rigorously tested *in vivo* before optimal effect of synergistic formulation could be achieved.

Materials and Methods

Materials

Absolute ethanol (>99.9%), acetic acid, AD-COOH, 2-aminoethythiol hydrochloride, 3-aminopropyltriethoxysilane, *Bcl-2* primary antibody (Mouse), bovine serum albumin (BSA), cetyltrimethylammonium bromide (CTAB, 90%), DAPI, DCC, diethyl ether, DMF (99%), MTT, 2,2′-dithiodipyridine, DTT, Dox, DMEM, fetal bovine serum (FBS), FITC, formaldehyde, GSH, hydrochloride (HCl, assay 37%), *N*-hydroxylsuccinimide (NHS), Lipofectamine RNAiMAX reagent (Invitrogen), MPTMS, methanol (MeOH, 99.5%), PBS buffer, siRNA duplex against *Bcl-2* protein, sodium hydroxide (NaOH), TEOS (99%), tris-borate-ethylenediaminetetraacetic acid (TBE) buffer, β-tubulin primary antibody (Rabbit) and secondary antibody (goat anti-mouse and goat anti-rabbit), and universal siRNA negative control were purchased commercially.

Instruments

FESEM and TEM images were captured by FESEM 6340 at 5 kV and JEOL 2010 TEM at 200 kV, respectively. XRD pattern was collected by low-angle X'Pert XRD from $2\theta=1.5$ to 8. Zeta potential values were measured by MavernNanosizer, and each sample was measured thrice for statistic analysis. Surface area and pore size distribution of MSNP-SH were characterized by ASAP-2020 Mircomeritics. FT-IR spectra were measured through Fourier transformed infrared spectrometer. ^{13}C solid state NMR spectrum of MSNP-SS-AD was carried out by 400 MHz JEOL ECA400 with cross polarization magic angle spinning probe. *In vitro* release test was monitored by RF-5301 fluorophotometer. Nanodrop 1.0 was used to determine the siRNA concentration. UV-vis absorption was measured by UV-vis 2501 Spectrometer. Agarose gel electrophoresis was performed by ENDRO GEL XL E0160 electrophoresis system. A microplate reader (infinite 200 PRO; Tecan) was used for the MTT assay. CLSM images of transfected HeLa cells were taken by a confocal fluorescence microscope (Leica TCS SP5, 40×oil objective). Flow cytometry data were collected by BD FACS Calibur Flow Cytometer. *In vivo* images of transgenic zebrafish larvae were acquired with an upright Zeiss Axiovert 200M laser scanning microscope (LSM) Meta 510 (Carl Zeiss), equipped with a×40 numerical aperture and 0.75 W

Achroplan long working distance dipping objective. Bright field zebrafish images were acquired with Olympus AX70 upright compound microscope attached to a ProgRes C10 plus digital camera (JENOPTIK Laser, Optik, Systeme GmbH).

MSNP-SH

MSNP-SH was prepared by a cocondensation method in base solution to obtain uniform surface distribution of the functional groups. In a typical synthetic procedure, CTAB (500 mg) was dissolved in distilled H_2O (250 ml). NaOH aqueous solution (1.75 ml, 2 *M*) was added into the above solution. The mixture solution was heated to 80°C under vigorous stirring. When the temperature was stabilized, TEOS (2.5 ml) was slowly added into the mixture solution. MPTMS (0.5 ml) was added dropwise after 15 min. The mixture solution was stirred at 80°C for another 2 h. As for FITC labeled nanoparticles, FITC (1.3 mg) was dissolved in absolute ethanol (1.5 ml) containing 3-triethoxysilylpropylamine (3 μl), and the mixture solution was gently stirred for 2 h in the dark before adding into TEOS (2.5 ml). Then, the formed nanoparticles were collected by centrifugation at 8000 rpm for 10 min and washed with MeOH and distilled H_2O. Surfactant was removed by suspending the thiol group functionalized silica nanoparticles in MeOH (50 ml) containing condensed HCl (3 ml, 37%) and refluxing at 80°C for 24 h. MSNP-SH was collected by centrifugation and thoroughly washed with MeOH and distilled H_2O. The nanoparticles were dried in vacuo at 80°C for 24 h.

S-*(2-Aminoethylthio)-2-thiopyridine hydrochloride*

The preparation of the compound was according to a previous literature report (11).

MSNP-SS-NH$_2$

Disulfide bond formation on the nanoparticle surface was realized by suspending MSNP-SH (200 mg) in MeOH (30 ml) followed by the addition of SATH (200 mg). The mixture solution was stirred at room temperature for 24 h. MSNP-SS-NH_2 formed was collected by centrifugation, thoroughly washed with MeOH and distilled H_2O, and dried in vacuo at 80°C for 24 h.

MSNP-SS-AD

AD-COOH (225 mg) was dissolved in DMF (10 ml) containing DCC (645 mg) and NHS (360 mg). After the mixture solution was stirred for 2 h, a DMF (5 ml) solution containing fully suspended MSNP-SS-NH_2 (100 mg) was added. After reacting for 24 h, MSNP-SS-AD was collected by centrifugation and washed with DMF, MeOH, and distilled H_2O extensively.

CD-2NH$_2$

Ethylenediamine-modified β-CD derivative was prepared according to a previous report (58). Seven ethylenediamine groups were covalently linked at the primary side of the β-CD ring.

Drug loading and controlled release test

RhB or Dox was loaded into the nanoparticles by stirring aqueous solution (1 ml) containing either RhB or Dox (1 mg) and MSNP-SS-AD (10 mg) at room temperature for 24 h. Then, β-CD or CD-2NH_2 (5 mg) was added into the solution to cap the mesopores by forming the host–guest complex between AD and β-CD on the nanoparticle surface. After stirring the solution for 5 h, the nanoparticles were collected by centrifugation at 13,000 rpm for 10 min and washed with distilled H_2O for three times. The collected nanoparticles were suspended in PBS buffer (5 ml, pH 7.4) as stock solution ($2\,mg\cdot ml^{-1}$) for future tests. The loading amount of the drugs was calculated by comparing the UV-vis absorption at 553 nm for RhB and 485 nm for Dox. Controlled release experiments were conducted by adding as-prepared stock solution (500 μl) into PBS buffer (500 μl, pH 7.4) with or without the reducing agent GSH or DTT. The solution was centrifuged at 13,000 rpm for 3 min, and fluorescence intensity ($\lambda_{ex/em}$ = 510/572 nm for RhB, $\lambda_{ex/em}$ = 485/553 nm for Dox) of the supernatant was recorded to monitor the kinetic release process of each sample. The final fluorescence intensity after 24 h was regarded as complete release (100%). For each sample, three independent experiments were carried out for statistic analysis.

Agarose gel electrophoresis

MSNP-SS-AD (1 mg) was mixed with CD-2NH_2 (1 mg) in aqueous solution, and the mixture was stirred for 5 h. CD-2NH_2-capped MSNP-SS-AD (MSNP-SS-AD + CD-2NH_2) was collected by centrifugation and excess CD-2NH_2 was removed by washing the nanoparticles thrice with distilled H_2O. Then, MSNP-SS-AD + CD-2NH_2 was suspended in distilled H_2O (1 ml, $2\,mg\cdot ml^{-1}$). siRNA duplex against *Bcl-2* protein, *Bcl-2* siRNA, was used in agarose gel electrophoresis. Proper amount of *Bcl-2* siRNA solution ($0.2\,\mu g\cdot\mu l^{-1}$) and MSNP-SS-AD + CD-2$NH_2$ solution ($2\,mg\cdot ml^{-1}$) were mixed to obtain different nanoparticle-to-siRNA(+) weight ratios. Free *Bcl-2* siRNA without the nanoparticles was placed in the first lane as the control. In the second line, only MSNP-SS-AD + CD-2NH_2 was added. To demonstrate that the siRNA(+) release is induced by the disulfide bond cleavage, DTT (50 m*M*) was added into the last lane with the highest nanoparticle-to-siRNA(+) weight ratio of 110:1. Proper amount of distilled H_2O was added into each lane to keep the concentration of siRNA(+) constant. MSNP-SS-AD + CD-2NH_2 was incubated with siRNA(+) for 1 h before running the electrophoresis. The agarose gel electrophoresis was carried out in agarose gel (1.5 wt%) within TBE buffer at 100 V for 15 min.

Cell culture

HeLa cells were cultured in DMEM containing 10% FBS and nonessential amino acids (0.1 m*M*). The culture was maintained at 37°C in a humidified atmosphere containing 5% CO_2.

Bcl-2 *gene knockdown and Western blot assay*

siRNA duplex sequence against *Bcl-2* protein, noted as siRNA(+), was presented as follows: sense strand 5′-rGrUr ArCrArUrCrCrArUrUrArUrArArGrCrUrGrUrCrGrCdAdG-3′, antisense strand 5′-rUrGrCrGrArCrArGrCrUrUrArUrAr ArUrGrGrArUrGrUrArCrUrU-3′. Non-targeting siRNA duplex, noted as siRNA(−), was used as the negative control. HeLa cells were seeded into six-well plate at a density of

20×10^4 cells/well in complete DMEM and grown for 24 h. Fresh DMEM without any antibiotics and FBS was used for the gene knockdown experiments. CD-2NH_2-capped MSNP-SS-AD (MSNP-SS-AD + CD-2NH_2, 50 μl, 2 mg·ml^{-1}) was mixed with either siRNA(+) or siRNA(−) (5 μl, 0.2 μg·μl^{-1}), and the mixture was incubated for 2 h with gentle stirring every 20 min. The CD-2NH_2-capped MSNP-SS-AD/siRNA complex (MSNP-SS-AD + CD-2NH_2 + siRNA) with a nanoparticle-to-siRNA weight ratio of 110:1 was stabilized by BSA (1 mg·ml^{-1}) before adding fresh medium (445 μl). For siRNA transfection by Lepofectamine as the positive control, same amount of siRNA(+) was used according to the product instruction of Lipofectamine RNAiMAX reagent. Free siRNA(+) (5 μl, 0.2 μg·μl^{-1}) and MSNP-SS-AD + CD-2NH_2 (50 μl, 2 mg·ml^{-1}) were added into fresh medium (495 and 450 μl), respectively. In total, each sample was prepared in the same volume (500 μl). The cell culture medium in the six-well plate was removed and the prepared sample (500 μl) was added. After 16 h exposure, the medium in each well was replaced by fresh complete DMEM (2 ml), and HeLa cells were incubated for another 56 h. Then, the cell culture medium was removed and the cells were washed with chilled PBS buffer (pH 7.4) for three times. After adding lysis buffer (500 μl), the plate was shaken at 4°C for 30 min to break cell membranes. The lysis buffer was collected and centrifuged (13 rpm, 4°C) for 10 min, and the supernatant was then collected. The protein concentration was quantified by Pierce BCA Protein Assay Kit according to its product instruction. Relative *Bcl-2* protein expression level was checked by western blot assay using β-tubulin as internal standard, which was performed according to its standard protocol.

MTT cytotoxicity assay

The cytotoxicity was evaluated by employing MTT assay. Equivalent amount of free Dox was used in the cytotoxicity experiments as the control. HeLa cells were seeded into 96-well plate at a density of 1×10^4 cells/well in complete DMEM and grown for 24 h. Then, each medium was changed into complete DMEM containing free Dox (2.5 μg·ml^{-1}), CD-2NH_2-capped MSNP-SS-AD (MSNP-SS-AD + CD-2NH_2), Dox-loaded CD-2NH_2-capped MSNP-SS-AD (MSNP-SS-AD + Dox + CD-2NH_2), Dox-loaded CD-2NH_2-capped MSNP-SS-AD/siRNA(+) complex [MSNP-SS-AD + Dox + CD-2NH_2 + siRNA(+)] with a nanoparticle-to-siRNA weight ratio of 110:1, and Dox-loaded CD-2NH_2-capped MSNP-SS-AD/siRNA(−) complex [MSNP-SS-AD + Dox + CD-2NH_2 + siRNA(−)] with a nanoparticle-to-siRNA weight ratio of 110:1, respectively. An equivalent amount of MSNP-SS-AD concentration (50 μg·ml^{-1}) was used in each sample. After 16 h exposure, the medium in each well was replaced by fresh complete DMEM (100 μl). MTT assay was conducted after 56 h incubation. The medium in each well was changed into medium containing MTT (100 μl, 0.5 mg·ml^{-1}). After incubation for 4 h, the medium was removed and dimethyl sulfoxide (100 μl) was added into each well. The plate was gently shaken for 15 min and absorbance intensity at 560 nm was recorded using a microplate reader (infinite 200 PRO; Tecan). The relative cell viability related to control wells that were only treated with medium was calculated by $[A]_{test}/[A]_{control}$, where $[A]_{test}$ and $[A]_{control}$ are the average absorbance of the test and control samples, respectively.

Confocal laser scanning microscopy

HeLa cells were seeded in 35 mm plastic-bottomed μ-dishes and grown in complete DMEM for 24 h. Then, HeLa cells were treated with FITC-labeled MSNP-SS-AD, CD-2NH_2-capped MSNP-SS-AD (MSNP-SS-AD + CD-2NH_2), and Dox-loaded CD-2NH_2-capped MSNP-SS-AD (MSNP-SS-AD + Dox + CD-2NH_2), respectively, under an equivalent amount of MSNP-SS-AD concentration (50 μg·ml^{-1}). After 24 h incubation, the medium was removed and the cells were washed thrice with PBS buffer (pH 7.4) and fixed with 4.0% formaldehyde at room temperature for 15 min. After removing 4.0% formaldehyde and washing with PBS buffer (pH 7.4) thrice, the cell nucleus was stained with DAPI (1 μg·ml^{-1}) for 15 min and washed with PBS buffer (pH 7.4) thrice before capturing the CLSM images using a confocal microscope (Leica TCS SP5, 60× oil objective).

Flow cytometry analysis

HeLa cells were seeded in six-well plate and grown for 24 h. Then, the cells were treated with FITC labeled MSNP-SS-AD, CD-2NH_2-capped MSNP-SS-AD (MSNP-SS-AD + CD-2NH_2), Dox-loaded CD-2NH_2-capped MSNP-SS-AD (MSNP-SS-AD + Dox + CD-2NH_2), respectively, under an equivalent amount of MSNP-SS-AD concentration (50 μg·ml^{-1}), and also treated with equivalent amount of free Dox. After 24 h incubation, the cells were washed by PBS thrice and collected by trypsin. The flowcytometry analysis was performed after washing the collected cells with PBS by centrifugation. The flow cytometry data were collected by BD FACSCalibur Flow Cytometer.

Zebrafish care and maintenance

Wild-type and transgenic zebrafish lines TG(fli1:EGFP), SqKR19, Et(krt4:EGFP)sqet33e20 (or SqET33-e20), and Krasv^{12} were maintained in the Institute of Molecular and Cell Biology zebrafish facility. The embryos were obtained and the experiments were carried out according to the Institutional Animal Care and Use Committee, Agency for Science, Technology and Research, Singapore (IACUC) rules and regulations (the Biopolis IACUC application No. 090430). To prevent the formation of melanin and to ensure optical translucence of transgenic larvae for confocal imaging, 1-phenyl-2-thiourea was added to zebrafish embryos at 22 hpf.

Brain-targeted microinjection of CD-2NH_2-capped MSNP-SS-AD

36 hpf or 3-day-old transgenic larvae were first immobilized, dorsal side up, in 1% UltraPure™ low melting point agarose (Invitrogen). CD-2NH_2-capped MSNP-SS-AD (6 nl, 0.4 μg·μl^{-1}) was then microinjected into the brain ventricle. Microinjected zebrafish larvae and non-injected control were grown in an incubator under 28.5°C.

Pericardial microinjection of free Dox or Dox-loaded CD-2NH_2-capped MSNP-SS-AD

For microinjection into the zebrafish circulation, 3-day-old TG(fli1:EGFP) larvae (32) were mounted ventral side up in 1% molten low melting agarose, and Dox (250 μg·ml^{-1}) or Dox-loaded CD-2NH_2-capped MSNP-SS-AD (10 mg·ml^{-1}) was injected into the sinus venosus of transgenic zebrafish larvae.

Abdominal microinjection of Dox-loaded CD-2NH$_2$-capped MSNP-SS-AD

For microinjection into the vicinity of liver tumor (45), 4-day-old transgenic zebrafish experiencing liver hyperplasia was mounted ventral side up in 1% UltraPure low melting point agarose (Invitrogen), and Dox-loaded CD-2NH$_2$-capped MSNP-SS-AD ($10\,mg\cdot ml^{-1}$) was injected into the site of the abdomen near the liver without injuring the tissue.

Whole mount in situ *hybridization*

Embryos at 3 dpf were processed for WISH using a technique that was described previously (40). Dig-labeled (Roche Applied Science) antisense EGFP RNA probe was used for this analysis. Images were taken using Olympus AX70 upright compound microscope attached to a ProgRes C10 plus digital camera (JENOPTIK Laser, Optik, Systeme GmbH), and the stained EGFP-positive area was quantified using the Image J software. A quantitative measurement of interference with GFP expression was assessed using WISH to detect choroid plexus expressing EGFP. The stained EGFP-positive area was quantified using the Image J software.

Formulations of CD-2NH$_2$-capped MSNP-SS-AD complexed with siRNA for brain-targeted injections

siRNA duplex targeting EGFP (CAA GCU GAC CCU GAA GUU CTT) was purchased from Integrated DNA Technologies, Inc. Condition 1 (C1): $0.04\,\mu g\cdot\mu l^{-1}$ of siRNA against GFP; Condition 2 (C2): $0.12\,\mu g\cdot\mu l^{-1}$ CD-2NH$_2$-capped MSNP-SS-AD with $0.04\,\mu g$ of siRNA against GFP, 3:1; Condition 3 (C3): $0.2\,\mu g\cdot\mu l^{-1}$ CD-2NH$_2$-capped MSNP-SS-AD with $0.04\,\mu g$ of siRNA against GFP, 5:1; and Condition 4 (C4): $0.4\,\mu g\cdot\mu l^{-1}$ CD-2NH$_2$-capped MSNP-SS-AD with $0.04\,\mu g$ of siRNA against GFP, 10:1.

In vivo *imaging of transgenic zebrafish larvae*

Transgenic larvae were mounted in 1% UltraPure low melting point agarose prior to imaging. Confocal microscopy images of living transgenic larvae were acquired with an upright (Zeiss Axiovert200M) laser scanning microscope (LSM Meta 510; Carl Zeiss) using two laser lines (30 mW Argon and 1 mW HeNe) as the excitation source to visualize GFP and internalized Dox and using the 505/530 nm and 560/615 nm emission band-pass filters, respectively. Images were acquired under the same acquisition settings, for all imaged larvae.

Acknowledgments

This work was financially supported by the Singapore National Research Foundation Fellowship (NRF2009NRF-RF001-015), the Singapore National Research Foundation CREATE program—Singapore Peking University Research Centre for a Sustainable Low-Carbon Future, and the Centre of Excellence for Silicon Technologies (A*Star SERC No. 112 351 0003). We thank Alexander Emelyanov for providing transgenic zebrafish with mifepristone-inducible kras^{v12} expression in the liver.

Author Disclosure Statement

No competing financial interests exist.

References

1. Aliabadi HM, Landry B, Sun C, Tang T, and Uludag H. Supramolecular assemblies in functional siRNA delivery: where do we stand? *Biomaterials* 33: 2546–2569, 2012.
2. Ambrogio MW, Thomas CR, Zhao YL, Zink JI, and Stoddart JF. Mechanized silica nanoparticles: a new frontier in theranosticnanomedicine. *Acc Chem Res* 44: 903–913, 2011.
3. Bhattarai SR, Muthuswamy E, Wani A, Brichacek M, Castañeda AL, Brock SL, and Oupicky D. Enhanced gene and siRNA delivery by polycation-modified mesoporous silica nanoparticles loaded with chloroquine. *Pharm Res* 27: 2556–2568, 2010.
4. Burkett SL, Sims SD, and Mann S. Synthesis of hybrid inorganic–organic mesoporous silica by co-condensation of siloxane and organosiloxane precursors. *Chem Commun* (11): 1367–1368, 1996.
5. Chen AM, Zhang M, and Wei D. Co-delivery of doxorubicin and *Bcl-2* siRNA by mesoporous silica nanoparticles enhances the efficacy of chemotherapy in multidrug-resistant cancer cells. *Small* 5: 2673–2677, 2009.
6. Cleary ML, Smith SD, and Sklar J. Cloning and structural analysis of cDNAs for bcl-2 and a hybrid bcl-2/immunoglobulin transcript resulting from the t(15;19) translocation. *Cell* 47: 19–28, 1986.
7. Cory S, and Adams JM. The Bcl2 family: regulators of the cellular life-or-death switch. *Nat Rev Cancer* 2: 647–656, 2002.
8. Cotton M, Wangner E, Zatloukal K, Phillips S, Curiel DT, and Birnstiel ML. High-efficiency receptor-mediated delivery of small and large 48 kilobase gene constructs using the endosome-disruption activity of defective or chemically inactivated adenovirus particles. *Proc Natl Acad Sci U S A* 89: 6094–6098, 1992.
9. Cromwell W, Bystrom K, and Eftink M. Cyclodextrin-adamantanecarboxylate inclusion complexes: studies of the variation in cavity size. *J Phys Chem* 89: 326–332, 1985.
10. de Fougerolles A, Vornlocher HP, Maraganore J, and Lieberman J. Interfering with disease: a progress report on siRNA-based therapeutics. *Nat Rev Drug Discov* 6: 443–453, 2007.
11. Ebright YW, Chen Y, Kim Y, and Ebright RH. S-[2-(4-Azidosalicylamido)ethylthio]-2-thiopyridine: radioiodinatable, cleavable, photoactivatible cross-linking agent. *Bioconjug Chem* 7: 380–384, 1996.
12. Elbashir SM, Harborth J, Lendeckel W, Yalcin A, Weber K, and Tuschl T. Duplexes of 21-nucleotide RNAs mediate RNA interference in cultured mammalian cells. *Nature* 411: 494–498, 2001.
13. Eytan GD. Mechanism of multidrug resistance in relation to passive membrane permeation. *Biomed Pharmacother* 59: 90–97, 2005.
14. Fujita Y. Interface between normal and transformed epithelial cells: a road to a novel type of cancer prevention and treatment. *Cancer Sci* 102: 1749–1755, 2011.
15. Gabbay EJ, Grier D, Fingerle RE, Reimer R, Levy R, Pearce SW, and Wilson WD. Interaction specificity of the anthracyclines with deoxyribonucleic acid. *Biochemistry* 15: 2062–2070, 1976.
16. García-Lecea M, Kondrychyn I, Fong SH, Ye ZR, and Korzh V. *In vivo* analysis of choroid plexus morphogenesis in zebrafish. *PLoS One* 3: e3090, 2008.
17. Gartmann N, and Brühwiler D. Controlling and imaging the functional-group distribution on mesoporous silica. *Angew Chem Int Ed* 48: 6354–6356, 2009.
18. Giri S, Trewyn BG, Stellmaker MP, and Lin VSY. Stimuli-responsive controlled-release delivery system based on

mesoporous silica nanorods capped with magnetic nanoparticles. *Angew Chem Int Ed* 44: 5038–5044, 2005.
19. Goren D, Horowitz AT, Tzemach D, Tarshish M, Zalipsky S, and Gabizon A. Nuclear delivery of doxorubicin via folate-targeted liposomes with bypass of multidrug-resistance efflux pump. *Clin Cancer Res* 6: 1949–1957, 2000.
20. Hamilton AJ, and Baulcombe DC. A species of small antisense RNA in posttranscriptional gene silencing in plants. *Science* 286: 950–952, 1999.
21. Hannon GJ, and Rossi JJ. Unlocking the potential of the human genome with RNA interference. *Nature* 431: 371–378, 2004.
22. He QJ, Shi JL, Cui XZ, Zhao JJ, Chen Y, and Zhou J. Rhodamine B-co-condensed spherical SBA-15 nanoparticles: facile co-condensation synthesis and excellent fluorescence features. *J Mater Chem* 19: 3395–3403, 2009.
23. He QJ, Shi JL, Zhao JJ, Chen Y, and Chen F. Bottom-up tailoring of nonionic surfactant-templated mesoporous silica nanomaterials by a novel composite liquid crystal templating mechanism. *J Mater Chem* 19: 6498–6503, 2009.
24. Jabr-Milane LS, van Vlerken LE, Yadav S, and Amiji MM. Multi-functional nanocarriers to overcome tumor drug resistance. *Cancer Treat Rev* 34: 592–602, 2008.
25. Janát-Amsbury MM, Yockman JW, Lee M, Kern S, Furgeson DY, Bikram M, and Kim SW. Combination of local, nonviral IL12 gene therapy and systemic paclitaxel treatment in a metastatic breast cancer model. *Mol Ther* 9: 829–836, 2004.
26. Kecht J, Schlossbauer A, and Bein T. Selective functionalization of the outer and inner surfaces in mesoporous silica nanoparticles. *Chem Mater* 20: 7207–7214, 2008.
27. Kim H, Kim S, Park C, Lee H, Park HJ, and Kim C. Glutathione-induced intracellular release of guests from mesoporous silica nanocontainers with cyclodextrin gatekeepers. *Adv Mater* 22: 4280–4283, 2010.
28. Kishida T, Asada H, Itokawa Y, Yasutomi K, Shin-Ya M, Gojo S, Cui FD, Ueda Y, Yamagishi H, Imanishi J, and Mazda O. Electrochemo-gene therapy of cancer: intratumoral delivery of interleukin-12 gene and bleomycin synergistically induced therapeutic immunity and suppressed subcutaneous and metastatic melanomas in mice. *Mol Ther* 8: 738–745, 2003.
29. Korzh V, Teh C, Kondrychyn I, Chudakov DM, and Lukyanov S. Visualizing compound transgenic zebrafish in development: a tale of green fluorescent protein and KillerRed. *Zebrafish* 8: 23–29, 2011.
30. Kresge CT, Leonowicz ME, Roth WJ, Vartuli JC, and Beck JS. Ordered mesoporous molecular sieves synthesized by a liquid-crystal template mechanism. *Nature* 359: 710–712, 1992.
31. Larsen AK, Escargueila AE, and Skladanowski A. Resistance mechanisms associated with altered intracellular distribution of anticancer agents. *Pharmacol Ther* 85: 217–229, 2000.
32. Lawson ND, and Weinstein BM. *In vivo* imaging of embryonic vascular development using transgenic zebrafish. *Dev Biol* 248: 307–318, 2002.
33. Liong M, Lu J, Kovochich M, Xia T, Ruehm SG, Nel AE, Tamanoi F, and Zink JI. Multifunctional inorganic nanoparticles for imaging, targeting, and drug deliver. *ACS Nano* 2: 889–896, 2008.
34. Luo D, and Saltzman WM. Synthetic DNA delivery systems. *Nat Biotechnol* 18: 33–37, 2000.
35. Luo Z, Cai K, Hu Y, Li J, Ding X, Zhang B, Xu D, Yang W, and Liu P. Redox-responsive molecular nanoreservoirs for controlled intracellular anticancer drug delivery based on magnetic nanoparticles. *Adv Mater* 24: 431–435, 2012.
36. Luo Z, Cai K, Hu Y, Zhao L, Liu P, and Yang WH. Redox-responsive nanoreservoirs based on collagen end-capped mesoporous silica nanoparticles for targeted drug delivery. *Angew Chem Int Ed* 50: 640–643, 2011.
37. Ma Y, Zhang P, Wang F, Yang J, Yang Z, and Qin H. The relationship between early embryo development and tumourigenesis. *J Cell Mol Med* 14: 2697–2701, 2010.
38. Macquarrie DJ. Direct preparation of organically modified MCM-type materials. Preparation and characterisation of aminopropyl–MCM and 2-cyanoethyl–MCM. *Chem Commun* (16): 1961–1962, 1996.
39. Malone RW, Hickman MA, Lehmann-Bruinsma K, Sih TR, Walzem R, Carlson DM, and Powell JS. Dexamethasone enhancement of gene expression after direct hepatic DNA injection. *J Biol Chem* 269: 29903–29907, 1994.
40. McCaffrey LM, and Macara IG. Epithelial organization, cell polarity and tumorigenesis. *Trends Cell Biol* 21: 727–735, 2011.
41. Meister A, and Anderson ME. Glutathione. *Annu Rev Biochem* 52: 711–760, 1983.
42. Meng H, Liong M, Xia T, Li Z, Ji Z, Zink JI, and Nel AE. Engineered design of mesoporous silica nanoparticles to deliver doxorubicin and P-glycoprotein siRNA to overcome drug resistance in a cancer cell line. *ACS Nano* 4: 4539–4550, 2010.
43. Mimeault M, and Batra SK. Emergence of zebrafish models in oncology for validating novel anticancer drug targets and nanomaterials. *Drug Discov Today* 18: 128–140, 2013.
44. Minko T, Kopeckova P, and Kopecek J. Comparison of the anticancer effect of free and HPMA copolymer-bound adriamycin in human ovarian carcinoma cells. *Pharm Res* 16: 986–996, 1999.
45. Nguyen AT, Emelyanov A, Koh CH, Spitsbergen JM, Parinov S, and Gong Z. An inducible $kras^{V12}$ transgenic zebrafish model for liver tumorigenesis and chemical drug screening. *Dis Model Mech* 5: 63–72, 2012.
46. Saad M, Garbuzenko OB, and Minko T. Co-delivery of siRNA and an anticancer drug for treatment of multidrug-resistant cancer. *Nanomedicine* 3: 761–776, 2008.
47. Seyhan AA. RNAi: a potential new class of therapeutic for human genetic disease. *Hum Genet* 130: 583–605, 2011.
48. Shi JL, Hua ZL, and Zhang LX. Nanocomposites from ordered mesoporous materials. *J Mater Chem* 14: 795–806, 2004.
49. Szejtli J. *Cyclodextrin Technology*. Dordrecht, The Netherlands: Kluwer Academic Publishers, p. 464, 1988.
50. Torney F, Trewyn BG, Lin VSY, and Wang K. Mesoporous silica nanoparticles deliver DNA and chemicals into plants. *Nat Nanotechnol* 2: 295–300, 2007.
51. Tschuch C, Schulz A, Pscherer A, Werft W, Benner A, Hotz-Wagenblatt A, Barrionuevo LS, Lichter P, and Mertens D. Off-target effects of siRNA specific for GFP. *BMC Mol Biol* 9: 60, 2008.
52. Tsujimoto Y, Finger LR, Yunis J, Nowell PC, and Croce CM. Cloning of the chromosome breakpoint of neoplastic B cells with the t(14;18) chromosome translocation. *Science* 226: 1097–1099, 1984.
53. Vallet-Regi M, Ramila A, del Real RP, and Perez-Pariente J. A new property of MCM-41: drug delivery system. *Chem Mater* 13: 308–311, 2001.
54. Verma A, Simard JM, Worrall JWE, and Rotello VM. Tunable reactivation of nanoparticle-inhibited B-galactosidase by glutathione at intracellular concentrations. *J Am Chem Soc* 126: 13987–13991, 2004.

55. Wong HL, Bendayan R, Rauth AM, Xue HY, Babakhanian K, and Wu XY. A mechanistic study of enhanced doxorubicin uptake and retention in multidrug resistant breast cancer cells using a polymer-lipid hybrid nanoparticle system. *J Pharmacol Exp Ther* 317: 1372–1381, 2006.
56. Yan H, Teh C, Sreejith S, Zhu L, Kwok A, Fang W, Ma X, Nguyen KT, Korzh V, and Zhao YL. Functional mesoporous silica nanoparticles for photothermal-controlled drug delivery *in vivo*. *Angew Chem Int Ed* 51: 8373–8377, 2012.
57. Zhang XH, Collins L, Sawyer GJ, Dong XB, Qiu Y, and Fabre JW. *In vivo* gene delivery via portal vein and bile duct to individual lobes of the rat liver using a polylysine-based nonviral DNA vector in combination with chloroquine. *Hum Gene Ther* 12: 2179–2190, 2001.
58. Zhao YL, Li Z, Kabehie S, Botros YY, Stoddart JF, and Zink JI. pH-operated nanopistons on the surfaces of mesoporous silica nanoparticles. *J Am Chem Soc* 132: 13016–13025, 2010.

Address correspondence to:
Prof. Yanli Zhao
Division of Chemistry and Biological Chemistry
School of Physical and Mathematical Sciences
Nanyang Technological University
21 Nanyang Link
637371, Singapore
Singapore

E-mail: zhaoyanli@ntu.edu.sg

Date of first submission to ARS Central, November 28, 2012; date of final revised submission, July 29, 2013; date of acceptance, August 10, 2013.

Abbreviations Used

AD = adamantane
AD-COOH = adamantane-1-carboxylic acid
BET = Brunauer–Emmett–Teller
Bcl-2 = B-cell lymphoma 2
BSA = bovine serum albumin
CD = cyclodextrin
CD-2NH_2 = ethylenediamine-modified β-cyclodextrin
CLSM = confocal laser scanning microscopy
CP MAS NMR = cross polarization and magic angle spinning nuclear magnetic resonance
CTAB = cetyltrimethylammonium bromide
DAPI = 4′,6-diamidino-2-phenylindole
DCC = dicyclohexylcarbodiimide
dpf = days post fertilization
DMEM = Dulbecco's modified Eagle's medium
DMF = dimethylformamide
Dox = doxorubicin
DTT = dithiothreitol
FBS = fetal bovine serum
FESEM = field emission scanning electron microscopy
FITC = fluorescein isothiocyanate
Ft-Ir = Fourier transform infrared spectroscopy
GFP = green fluorescence protein
GSH = glutathione
HCL = hydrochloride
hpf = hours post fertilization
IACUC = Institutional Animal Care and Use Committee, Agency for Science, Technology and Research, Singapore
MeOH = methanol
MPTMS = 3-mercaptopyltrimethoxysilane
MSNPs = mesoporous silica nanoparticles
MSNP-SH = thiol group-containing MSNPs
MSNP-SS-AD = AD-functionalized MSNPs
MSNP-SS-NH_2 = amino group-terminated nanoparticles
MTT = 3-(4,5-dimethylthiazol-2-Yl)-2,5-diphenyltetrazolium bromide
NaOH = sodium hydroxide
NHS = *N*-hydroxylsuccinimide
PBS = phosphate buffered saline
RhB = rhodamine B
RNAi = RNA interference
SATH = *S*-(2-aminoethylthio)-2-thiopyridine hydrochloride
TBE = tris-borate-Ethylenediaminetetraacetic acid
TEM = transmission electron microscopy
TEOS = tetraethylorthosilicate
UV-vis = ultraviolet-visible
WISH = whole mount *in situ* hybridization
XRD = X-ray Diffraction

This article has been cited by:

1. Gauthier Marc A.. 2014. Redox-Responsive Drug Delivery. *Antioxidants & Redox Signaling* **21**:5, 705-706. [Abstract] [Full Text HTML] [Full Text PDF] [Full Text PDF with Links]
2. Chung Yen Ang, Si Yu Tan, Yanli Zhao. 2014. Recent advances in biocompatible nanocarriers for delivery of chemotherapeutic cargoes towards cancer therapy. *Organic & Biomolecular Chemistry* **12**, 4776. [CrossRef]